AD-A054 752 MASSACHUSETTS INST OF TECH CAMBRIDGE DEPT OF AERONAU--ETC F/G 1/3
EXPERIMENTAL INVESTIGATION OF GUST RESPONSE OF HINGELESS HELICO--ETC(U)
JUN 77 C A VEHLOW

UNCLASSIFIED NL

| OF 2
AD
A054752

(6) EXPERIMENTAL INVESTIGATION OF GUST RESPONSE OF HINGELESS HELICOPTER ROTORS.

(1) SC

by

(9) Master's thesis,

(10) CHARLES A. VEHLOW

B.S. United States Military Academy
(1968)

(11) Jun 77

(12) 105p.

SUBMITTED IN PARTIAL FULFILLMENT
OF THE REQUIREMENTS FOR THE
DEGREE OF

MASTER OF SCIENCE

at the

MASSACHUSETTS INSTITUTE OF TECHNOLOGY
(June 1977)

Signature of Author Charles A. Vehlow
Department of Aeronautics and Astronautics, May 12, 1977

Certified by Norman D. Ham
Thesis Supervisor

Accepted by R. H. Miller
Chairman, Departmental Graduate Committee

LB

EXPERIMENTAL INVESTIGATION OF GUST RESPONSE OF HINGELESS HELICOPTER ROTORS

by

CHARLES A. VEHLOW

Submitted to the Department of Aeronautics and Astronautics on 12 May 1977 in partial fulfillment of the requirements for the Degree of Master of Science.

ABSTRACT

The response to wind gusts of a 1/10-scale hingeless helicopter rotor model in hovering and forward flight is studied experimentally through wind tunnel testing.

The experimental program involving design, construction, and testing of a five-foot-diameter rotor utilizing either three NACA 0012 planform blades or one operable blade with two dummy blades is described. The rotor design is such that the torsional stiffness of the blade assembly as well as the blade chordwise center-of-gravity location can be varied during the various phases of the test. Wind tunnel testing incorporates the variation of wind tunnel speed and the application of variable frequency, sinusoidal waveform gusts.

The flap, lag, and torsional response of the rotor in its various configurations was measured and compared with theoretical predictions.

Thesis Supervisor: Norman D. Ham, Sc.D.

Title: Professor of Aeronautics and Astronautics

ACKNOWLEDGMENT

The research described in this thesis was supervised by Professor Norman D. Ham. The author would like to express his gratitude for the candid advice and counsel and skilled guidance provided by Professor Ham during all phases of the conception, design, production, and testing of the wind tunnel model. Deep appreciation is also conveyed to Mr. Masahiro Yasue, whose theoretical conceptions led to the development of the model, and whose many timely suggestions and discussions led to the successful test completion. A special thanks is also due Mr. Paul Bauer. His common sense approach to problem solving along with a keen awareness and innovative approach to engineering techniques greatly simplified all phases of the model development.

TABLE OF CONTENTS

TABLE OF CONTENTS CONTINUED

TABLE OF CONTENTS CONTINUED

TABLE OF CONTENTS CONCLUDED

LIST OF ILLUSTRATIONS

LIST OF ILLUSTRATIONS CONTINUED

LIST OF ILLUSTRATIONS CONCLUDED

LIST OF TABLES

1. INTRODUCTION

1.1 Background

The concept of hingeless helicopter rotors has for many years been an area of increased emphasis regarding design and production. The increased control power and damping due to the large moment which can be transferred directly to the aircraft, as well as the simplicity of design in the areas of production and maintenance have made this concept very attractive; however, the structural couplings associated with this concept must also be dealt with. More specifically, the response of hingeless rotors to vertical gusts while in forward flight must be understood and properly controlled.

Most recently a theory regarding the chordwise center-of-gravity shift as a gust alleviation method has been developed (Ref. 1). This theoretical development deals with cases of varying blade torsional stiffness and blade chordwise center-of-gravity location. The theory predicts that center-of-gravity shifts are a very effective and simple method of alleviating blade gust response. In a typical theoretical wind tunnel model blade with a Locke number of 2.65, a 5% center-of-gravity shift towards the leading edge, the gust frequency of .1/rev. and an advance ratio $\mu = 0.4$, the collective flapping and the longitudinal cyclic flapping are reduced by 7% and 18%, respectively. The same model with a more typical Locke number of 10 would show even greater reductions of 35% and 53%, respectively. Additionally, the theory predicts a torsionally soft blade achieves even more reduction in the gust response than the torsionally stiff blade. Finally, a center-of-gravity shift towards the leading edge also reduces

lag damping due to Coriolis force, and extreme care must be taken to avoid blade instability when a center-of-gravity shift is employed.

1.2 Objective

The objective of the program undertaken and summarized in this thesis involved the construction of a 1/10-scale hingeless helicopter rotor wind tunnel model to be used in the testing of the developed theory regarding the use of varying torsional stiffness and blade chordwise center-of-gravity shift as a means of alleviating gust response. Specifically, a model was constructed which allowed for variation of torsional stiffness and blade chordwise center-of-gravity location. The model was designed in a manner so that torsional stiffness could be varied while holding chordwise and flatwise stiffness constant. A wind tunnel test program was developed utilizing the Wright Brothers Wind Tunnel at the Massachusetts Institute of Technology located in Cambridge, Massachusetts. This wind tunnel possesses a gust generator which was suitable for the gust simulation that was used during the testing program. The construction and validation tests were performed first on a three-bladed model employing standard torsion. The wind tunnel was run at two different speeds and the gust frequency was also varied. The tests continued on a three-bladed rotor utilizing two dummy blades with only a single operable blade. In this configuration, a chordwise center-of-gravity shift was applied to the single blade while minimal risk was imposed upon the entire rotor system. Variation was also made to the torsional stiffness, changing from the standard configuration to a soft torsion configuration.

2. MODEL DESIGN AND CONSTRUCTION

2.1 Overall Description and Design Considerations

In order to accurately test the theory and attempt to validate the developments as specified in the previous section, it was necessary to construct a hingeless helicopter rotor wind tunnel model. This model was to have certain variable parameters, those being variable torsional stiffness while maintaining constant chordwise and flatwise stiffness, and a variable center-of-gravity location for the model blades. It was decided to eliminate cyclic pitch control during the initial testing of this model in order that model construction could be accomplished more rapidly and economically. Based upon existing facilities at the Wright Brothers Wind Tunnel and proposed construction of the model, the parameters of wind tunnel speed, model shaft angle, and gust generator frequency were also quantities which could be varied depending upon desired flight configurations. Additionally, because of the orientation of the gust generator and its production of lateral gusts in the wind tunnel, it was decided that the model would be vertically oriented so as to maximize the effects of the lateral gust. This orientation will be described in greater detail in a later subsection. A complete description of all model parameters is given in Table 1.

2.1.1 Blades

The design of the hingeless helicopter model was completed using many parts and accessories already available at MIT. A three-bladed 1/10-scale model of a hingeless helicopter rotor was originally specified and is shown in Fig. 1. Blades that were used for the model incorporated a NACA 0012 section with a 21.2-inch reinforced fiberglass span possessing

two aluminum tubes and fiberglass covering over the 2-inch chord (Fig. 2). The aluminum tubes were present to carry fluid for smoke generation in other blades and thus served only to equalize blade weight and as such provided no structural support. Each blade had 8 deg. of linearly decreasing twist from root to tip. Each blade was to connect to the rotor hub by means of a metal flexure. Additionally, each blade was to have the capability of varying its center-of-gravity location. The metal flexure and the center-of-gravity variation will be discussed in greater detail in the following subsections.

Having determined the blade center-of-gravity and elastic axis locations, it was necessary to determine the stiffness characteristics of the blades. To accomplish this, a procedure utilizing the cantilevered blade, a series of weights, and optical lever and simple beam theory was developed. By beam theory, the following relationship exists:

$EI \frac{d\theta}{dx} = M$ where $M = (W)(\ell)$ $\quad$ W = Weight, ℓ = Station length from tip

Therefore

$$EI\frac{d\theta}{dx} = W\ell$$

Numerically, determine $d\theta/dx$ knowing the θ value at each station.

$$\frac{d\theta}{dx} = \frac{y_{i+1} - y_i}{x_{i+1} - x_i} + \frac{y_{i+2} - y_i}{x_{i+2} - x_i} - \frac{y_{i+2} - y_{i+1}}{x_{i+2} - x_{i+1}} \qquad \text{At end point } i = 1$$

$$\frac{d\theta}{dx} = \frac{y_i - y_{i-1}}{x_i - x_{i-1}} + \frac{y_{i+1} - y_i}{y_{i+1} - x_i} - \frac{y_{i+1} - y_{i-1}}{x_{i+1} - x_{i-1}} \qquad \text{At midpoints } i = 1 \text{ to } n - 1$$

$$\frac{d\theta}{dx} = \frac{y_n - y_{n-1}}{x_n - x_{n-1}} + \frac{y_n - y_{n-2}}{x_n - x_{n-2}} - \frac{y_{n-1} - y_{n-2}}{x_{n-1} - x_{n-2}} \qquad \text{At end point } i = n$$

Then $EI = \frac{W\ell}{d\theta/dx}$. Solve for EI_F or EI_C.

Therefore, by varying the amount of weight applied at each blade station, by varying the station, and by noting the associated deflections, the flatwise and chordwise stiffness could be determined for each particular blade.

A similar procedure could be utilized regarding determination of the torsional stiffness (GJ) of the blade. Again by beam theory:

$GJ \frac{d\theta}{dx} = T$ where T = applied moment

Using the same numerical derivative formula as used for EI_F and EI_C and knowing the θ values for each station, determine $d\theta/dx$.

Knowing $\frac{d\theta}{dx}$ at each station, find GJ.

$GJ = \frac{T}{d\theta/dx}$

Therefore, by varying the applied movement and also by changing the station location along the blade span, it was possible to determine the blade torsional stiffness.

To aid in the detection of blade deflection, a front-surfaced mirror and a laser beam were used (Ref. 2). For torsional and flatwise determination, the mirror was placed on the elastic axis of the blade at each blade station. For chordwise determination, the mirror was placed on the leading edge of the blade. An optical lever was then used to detect small changes in blade deflection as shown in Figs. 3, 4, and 5. The angular change from the measured deflections is known through the relationship $d/r = \sin\theta$. But the reflected beam goes through 2θ. Therefore, the actual structural rotation, α, is

$\alpha = \frac{1}{2} \sin^{-1} \frac{d}{r}$ or $\alpha = \frac{d}{2r}$ (small angles)

It was now possible to determine the blade stiffness characteristics for each blade. Measured stiffness data is shown in Fig. 6. Based upon these stiffnesses, the metal flexures which would connect the rotor blades to the rotor hub were now designed.

2.1.2 Flexures

Having determined the stiffness characteristics of the blades, it was necessary to design a metal flexure which would connect the blades to the rotor hub and possess characteristics noticeably softer than those of the blade. The flexure characteristics were determined to be those shown in Fig. 7. Design criteria for the chordwise, flatwise, and torsional stiffnesses of the flexures was based on anticipated deflections of the flexure and prior design experience of the project advisor. Initial approximations of flexure stiffnesses was to be approximately 1/10 those of the model blade being used. With these characteristics specified, it was necessary to specify the physical shape and dimensions of the flexure.

2.1.2.1 Rectangular Section

The first shape specified for the model flexure was rectangular. By specifying the width and the thickness of the section, chordwise and flatwise stiffnesses could be determined. The torsional stiffness was then fixed, based upon the selected width and thickness. While close approximations to the desired stiffnesses were attainable with this scheme, it was discovered that the rectangular section presented problems with respect to exceeding the bending-stress limitation of steel and even stainless steel. This excessive motion can be seen in Fig. 8, which are graphs of the chordwise, flatwise and torsional mode shapes using the rectangular

section. Thus, this design was eliminated.

2.1.2.2 Tapered Section

The next design considered was an attempt to distribute some of the flexure flapping motion over more of the metal flexure. A tapered flexure, thicker at its root than at its tip was designed. While this was adequate for flatwise motion, it produced very difficult properties with which to deal concerning chordwise and torsional motion. Thus, this design was quickly eliminated because of lack of compatibility with the desired characteristics.

2.1.2.3 Double Tapered Section

The next design consideration involved a double tapered section - tapered from root to tip to equalize the flatwise bending as above, but also tapered from root to tip in the chordwise sense to again help alleviate some of the anticipated large material stresses and simplify some of the coupled flap-torsion motion. However, it was very difficult to make any design changes to this patterned section. Additionally, this design appeared to not easily lend itself to changing from standard to soft torsion or to being adapted for use in the existing parts. Thus, it too was eliminated.

2.1.2.4 Rectangular and Tapered Section with Snubbers

The next design included the previous designs of the rectangular and tapered section, but added a pair of snubbers. These snubbers, designed to fit above and below the actual flexure, were tapered from root to tip, somewhat shorter than the actual flexure, and specified so as to aid primarily

in flatwise bending. The chordwise and torsional stiffnesses were then direct properties of the actual flexure. However, this scheme also proved unworkable because although adequate for pure flatwise, chordwise, or torsional bending, the flexure produced nonlinearities in its properties when any of the three motions were coupled together. Because it was known that coupled motion would be present in the actual model, this design iteration was also eliminated.

2.1.2.5 Rectangular Star Pattern

The next design involved a flexure which appeared like two crossed rectangles. By specifying the thickness and height for each rectangle, the chordwise and flatwise properties were determined. The torsional characteristic is then a function of the two shared middle sections (Ref. 3). While initially quite attractive for the model design, this scheme also proved too unwieldy. While moderately difficult to manufacture and adapt to the model attachment scheme, it proved virtually impossible to easily change the flexure torsional properties as desired. Thus, this design too was ruled inadequate.

2.1.2.6 Final Design Selection

The final design selected proved to be a compromise between other design iterations considered. A rectangular section was selected; however, a flapping hinge was added at the flexure tip end. Thus, the actual flexure could be designed specifying only chordwise and torsional characteristics. All flapping motion was thereby eliminated from the actual flexure. Along with this design came the requirement for a means of detecting any flapping motion. Thus, a flapping sensor was also specified which could meet this

requirement. A picture of the actual instrumented flexure and the flapping cuff and hinge are shown in Fig. 9.

2.1.3 Rotor Hub

The rotor hub design for the 3-bladed hingeless wind tunnel model was accomplished with little difficulty. Utilizing existing parts for the connection pieces which would join the hub to the flexures, a hub which incorporated the ability of varying collective pitch was designed and machined from 17-4 PH stainless steel. The hub was fitted with a 1/4 x 3/16 keyway and two set-screws in order to insure positive connection with the rotor drive shaft. The rotor hub and its associated hardware are pictured in Figs. 1 and 10.

2.1.4 Flapping Cuff

Because of the flexure design modification necessitated in order to maintain the capability of varying torsional stiffness during the desired wind tunnel tests, a flapping cuff was added to the original model design. This part of the model allows the rotor blade to flap up or down independently of the metal flexure. Thus, one of the design constraint requirements placed upon the original flexure was eliminated. The flapping cuff then provided the point of application for the blade-flapping measurement device and for the attachment of the blade counterweights.

The cuff was designed to link the blade and the metal flexure by attaching securely to both of these fixtures. Since it was necessary that the blade could freely flap, the attachment point at the flexure end was fitted with ball bearings. These bearings also possessed extended inner

races. A stud bolt then passed through the bearings and the flexure. By tightening this bolt, a friction grip of the bearing inner race on the flexure end was achieved. This friction grip also "indexed" the stud bolt with respect to the flexure. The stud bolt was then fitted with a .005-inch piece of feeler stock which extended into a slot cut into the flapping cuff. The feeler stock became the flap sensing flexure. This flap sensing flexure was instrumented with strain gages and thus allowed for the determination of the blade flap angle and monitoring of blade position during the wind tunnel tests. The flapping flexure is shown with the mounted flapping cuff in Fig. 9.

While the strain gages on the flapping flexure functioned extremely well during the wind tunnel tests, there was a minor problem with the strain gage connector wires. As the model blades flapped up or down during the wind tunnel tests, a strain was placed on the hook-up wires leading from the strain gages to the lead-in wires at their small solder joint. In the process of soldering the wires together, the smaller strain gage hook-up wires were weakened by the heat of soldering. Thus, the additional strain on the hook-up wires resulting from the flapping blades would occasionally cause these connections to fatigue and fail at the solder joint. After isolating this problem area the first time, necessary repairs were made and the test sequence continued. Even after subsequent failures, it was determined that it would be easier to merely repair the minor damage as opposed to redesigning the flapping flexure.

Finally, the attachment point of the flapping cuff at the blade end also provided a place to secure the blade counterweights. These counterweights will be described in the next subsection.

2.1.5 Blade Counterweights

As shown in Fig. 9, each blade was fitted with two cylindrical blade counterweights. The purpose of these counterweights was to counteract the primarily horizontal mass distribution of the blade, otherwise known as the blade feathering moment of inertia. By applying the counterweights with a vertical orientation, this tended to equalize the otherwise prevalent horizontal feathering moment of inertia (Ref. 4). The counterweights were designed for use on the three bladed model before application of the blade dampers became necessary. They were not redesigned after the application of the dampers.

2.1.6 Blade Center-of-Gravity Location

As pointed out earlier, the object of the wind tunnel tests was to attempt to validate the theory developed concerning the reduction of blade bending motion due to a vertical gust utilizing a passive control measure such as blade chordwise mass unbalance. It was necessary to design a means whereby blades with different center-of-gravity locations could be tested. One means of accomplishing this would be to design and build rotor blades which actually had different center-of-gravity locations. This method, however, would have proved too costly and time consuming for the intended test series. Therefore, it was decided that through the addition of tip weights, placed along the leading edge of each blade and in the vicinity of the blade tip, the desired center-of-gravity shift would be accomplished.

The actual scheme used to apply the tip weight to the model blade is shown in Fig. 11. A sleeve, fashioned from type 304 stainless steel, was welded to a .468-inch I.D. stainless steel tube. The tube was drilled

along its length in various locations. A tungsten slug, weighing approximately 40 grams, was machined to slip inside the stainless steel tube. By securing the slug at any one of the predrilled holes in the tube, an appropriate shift of the chordwise center-of-gravity either fore or aft was achieved. The different positions allowed for chordwise CG variation ranged from 35% chord (most aft position) to the 18% chord (most forward position). Values of chordwise CG position versus slug location are shown in Table 2. The tip weight assembly was secured to the blade by means of three .190-inch diameter shoulder bolts. Prior to actual model testing with the tip mass applied, careful calculations were made to check the shear, bearing, and tension loads on the reinforced fiberglass blade span and on the tip weight metal sleeve. In the most severe case, that being the sleeve bearing, a safety factor of almost 7 existed between expected loading forces and allowable loading forces. Therefore, the construction of the tip weight assembly was completed and the wind tunnel tests conducted.

2.1.7 Blade Dampers

During the initial design, a possible requirement for blade lead-lag dampers was discussed. The final model configuration possessed only a .0009% lead-lag structural damping ratio. It was decided to proceed without lead-lag dampers in order to keep construction simple while at the same time hoping that the structural damping inherent in the system would suffice.

During preliminary rotor runup, it was discovered that lead-lag dampers would be required. Initial calculations showed a chordwise resonance to exist between model rotational speeds of 600-650 RPM. As this shaft

speed was approached, chordwise bending of the metal flexure due to blade gravity moment became very evident. Yield strength of the 17-7 PH metal flexure was at 200 ksi while fatigue limits for this material exist at 150 ksi. A safety limit of 45 ksi was established for chordwise bending and reached at a shaft speed of 610 RPM in the no-damper configuration. Because of the established safety limitations and not desiring to risk model damage at higher RPM's, it was necessary to terminate testing and redesign the model to include lead-lag dampers.

The dampers which were designed and constructed, employed a double action, double ended closed-loop hydraulic system. Maximum piston stroke was 0.5-inch. The original damper is shown in Fig. 12. A double-ended cylinder was chosen in order that the piston motion in either direction would displace the same volume of fluid. While the different fluids available offered varying degrees of viscosity, light machine oil with a viscosity of 100 in^2/sec was selected for use. Additionally, the hydraulic system was selected because its damping properties vary approximately as the piston velocity squared. The dampers were filled with light machine oil utilizing a hypodermic syringe. This enabled almost all trapped air to be eliminated from the system.

Two other types of dampers were considered for use, but were eliminated because of undesirable properties. A small, commercially available airpot dashpot was examined. This small, lightweight device with a glass cylinder and graphite piston initially seemed very attractive for adaptation to the model rotor. However, bench tests on this dashpot system revealed that in order to derive good damping characteristics, it was

necessary for the piston top to be very close to the bottom of the cylinder (i.e., a small volume of air in the chamber). However, this condition could not be satisfied by the model rotor configuration at the maximum predicted lead-lag motion of the blade. Thus, in order to allow for this maximum piston displacement, a much greater volume of air would have been required in the dashpot cylinder. This, however, destroyed the desired damping characteristics of the dashpot as the increased volume turned the dashpot into an air-spring. In effect, the air compressed rather than passed through the dashpot orifice. Thus, this system was undesirable.

A third damper used a neoprene tube secured to a metal attaching bracket with a movable metal rod passing through the neoprene tube. The system damping would be provided by the metal rod sliding through the neoprene tube. By compressing the neoprene slightly in its lengthwise orientation, the damping of the device could be increased. However, the damping characteristic of this device is that damping varies linearly as the velocity of the piston. Thus, because its damping is not as good as the hydraulic system, this viscous-shear system of damping was selected as an alternate to the hydraulic cylinders.

The hydraulic cylinders selected for use were mounted on the model by attaching ball swivel rod end connectors to the cylinder body and to one piston rod end. This allowed the damper to function properly while independent of the blade lead-lag orientation and independent of flexure torsional motion. A small slotted plate was included in the adaptation in order that the piston could be centered at its mid-point with the blade in its neutral position. In its final configuration, the hydraulic dampers provided a 3.5% damping ratio when attached to the model.

A change was made in the original damper design after the first series of wind tunnel tests. It was discovered that while rotating at operating RPM, the mass of the large ball swivel connector caused a noticeable steady state torsional displacement resulting in "twisting off" of the preset blade angle of attack. Therefore, in order to reduce this mass and some of its associated steady state torsional displacement, a smaller ball swivel connector manufactured by Superior Linkage Company was purchased and adapted to the damper. This lighter and more compact unit provided the model with the same damping characteristics as before, but because of its reduced mass resulted in only 1/3 the steady state torsional displacement. A picture of the redesigned damper configuration is shown in Fig. 13.

2.1.8 Dummy Blades

To test the theoretical chordwise center-of-gravity shift predictions, the system for actually shifting the chordwise CG of an individual blade was designed as described in Subsection 2.1.6. In order that no more than one blade of the model be subjected to this major modification, it was decided to construct two dummy blades to complete the three bladed model (Ref. 5). The dummy blades incorporated the same mass as a complete test blade/damper assembly and also possessed the same spanwise center-of-gravity. Each dummy blade was constructed from 0.75-inch drill rod with the root end machined to fit the model rotor hub and the remainder of the rod turned to a 0.625-inch diameter. Rod length of 14.0 inches was determined for the appropriate CG location and such that the rod weight would be slightly less than the total weight desired. The final rod was threaded (5/8 x 18 NF) in order that the small additional mass needed to

equalize the weight requirement could be easily added and at the same time securely positioned in order to satisfy the CG requirement. Figure 14 shows a photograph of a dummy blade and its balancing weight.

2.2 Mounting of Rotor Shaft in Wind Tunnel

2.2.1 Horizontal Mounting

Early in the design development of the hingeless rotor model, it was decided that the model would be mounted with a vertical orientation in the test section of the Wright Brothers Wind Tunnel. The main reason for this decision was because of the availability of a lateral (or horizontal) gust which could be generated in the wind tunnel. The details of the gust generator and its associated equipment are explained in detail in Ref. 6. While this mounting orientation initially posed some problems, the solution and final mounting scheme provided a very adequate means for conducting the wind tunnel tests.

The Wright Brothers Wind Tunnel, built in 1939, contains a working balance in the test section. This balance has the capability of measuring lift, drag, and side-force components on a wind tunnel model,as well as possessing a turntable which allows for various angular orientations of a model with regard to the tunnel wind. By using the front trunnions of the wind tunnel balance, it was possible to design a pair of attachment points whereby the thrust produced by the rotor would appear as a side-force with regard to balance measurement. Additionally, by merely rotating the turntable of the balance, the rotor model shaft angle could be varied in order to simulate various forward flight configurations.

By using a series of guidelines, the model setup was also

strengthened against possible oscillatory loads which could develop during the gust generation. Thus, the balance provided an excellent attachment point in the wind tunnel for measuring rotor thrust, allowed for ease of shaft orientation, and provided structural strength to the entire model setup. A series of pictures showing the model mounted in the wind tunnel are included in Figs. 15 and 16.

In order to accommodate the rotor drive system, it was necessary to modify and rebuild some of the steel support structure outside of the Wright Brothers Wind Tunnel test section. This work was accomplished using 7.0-inch and 4.0-inch steel I beams and U channels. These modifications provided the rigid steel platform upon which the hydraulic motor and slip-ring assembly of the model were mounted. It also provided access areas for working on and controlling this equipment during the actual wind tunnel tests.

2.2.2 Splined Ball Coupling

Because of the desire to measure rotor thrust with minimal friction interference from a shaft-to-motor coupling, a double-universal-jointed, splined ball coupling was selected. This coupling in its attached configuration is shown in Fig. 17. The coupling was particularly useful for a number of reasons. Because of its patented spline ball design, it allowed for lateral movement of the rotor shaft while imposing only minimal friction forces upon the shaft; thus the thrust forces measured by the wind tunnel balance could be considered to be very close to those actually produced by the rotor. Next, the coupling allowed for a constant velocity to be maintained on the rotor shaft. This is important for the testing of the

model. Finally, by having a double universal coupling, flexibility regarding possible vertical misalignment, horizontal misalignment, or angular misalignment of the rotor shaft and the drive rotor was obtained. While all measures were taken to insure no misalignment, the splined ball coupling compensated for any undetected shortcoming that might have existed.

The requirement for shaft support at the connection end was provided by a linear ball-bushing bearing. This type of device was selected because its linear balls offered minimal friction opposition regarding lateral shaft movement, while at the same time it possessed a roller bearing assembly which could adequately absorb and withstand the rotational loads and forces imposed by running the shaft at 955 RPM.

2.3 Hydraulic Motor and Slip-Ring Assembly

To provide the means of turning the model helicopter rotor, a hydraulic motor fitted to a series of slip rings was utilized. A schematic of the pump assembly is shown in Fig. 18 with a picture of the actual hydraulic motor and slip-ring assembly shown in Fig. 19. The hydraulic motor is a Vickers hydraulic motor, rated at 3000 psi and a 1.52 cubic-inch/revolution-flow capacity. The speed of the rotor was controlled by means of a screwed bonnet regulating valve located at the control panel. The speed of the rotating shaft was monitored by means of a frequency counter which was connected to a 1/rev pulser on the slip-ring assembly. Precise variation of the RPM was attainable by either opening or closing the hydraulic control valve as necessary.

The slip-ring assembly utilized contained 31 usable rings with each ring possessing three (3) contact brushes. By using the three

contact brushes, the possibility of contact resistance variations and possible faulty signal transmission was minimized. The entire hydraulic motor and slip-ring assembly was disassembled, cleaned, reassembled and thoroughly checked for proper operation prior to conducting any wind tunnel tests. The system proved very reliable during the actual testing.

In order to pass the electrical excitation signal to the model and receive the output signal back at the control panel, it was necessary to modify the wiring of the original slip-ring assembly and design and wire an electrical system for this specific configuration. Because of the requirements for varying shaft angle and thus the necessity of much connection and reconnection of electrical leads during the experiment, the ability to quickly and easily connect and reconnect all electrical leads was desired. A fourteen pin and socket connector with jack screws was selected for use. These connectors were mounted on a shaft collar at the hub end of the rotor shaft and also at the hydraulic motor end. They provided the flexibility for connection/reconnection but at the same time were a very positive method of passing the electrical signal.

2.4 Controllers and Recording Devices

2.4.1 Strain-Gage Equipment

Having determined the model design and the desired measurable parameters, the electrical control mechanisms and data acquisition devices were selected and obtained. A 20-channel strain-gage amplifier was used to provide the 5 volt dc strain-gage excitation as well as the output amplification for each strain-gage bridge from the model. A schematic of the amplifiers is shown in Fig. 20. Each flexure was instrumented with

strain gages in order to detect chordwise bending and torsional motion. A diagram of a strain-gage bridge is shown in Fig. 21 while the mounted bridges are shown in Fig. 22. In addition, to detect the blade flapping motion, each flapping cuff flexure was instrumented with strain gages as is shown in Fig. 9. While the torsional, chordwise and flapping motion data of only one blade was actually recorded, the backup capability provided by the two other instrumented blades in the three-bladed configuration proved invaluable for recording data and for output comparison during the actual tests. As can be seen in Fig. 20, by varying the output resistor, the gain of each amplifier can be adjusted. A gain of 200 was selected for the chordwise bending motion, while a gain of 1000 was selected for torsional motion so as to provide increased sensitivity. The flapping gain was adjusted to 200. Once the strain gages were implaced, each flexure was calibrated using a simple bench test deflection technique. The calibration results are shown in Fig. 23.

2.4.2 Frequency Counters

Frequency counters were used to measure the RPM of the rotating model rotor shaft and the gust generator frequency. Since no tachometer was built into the model rotor shaft but a 1/rev signal was available on one of the slip rings, this ring was used to provide the signal for the RPM frequency counter. By making small adjustments of the hydraulic motor control valve, the speed of the shaft was accurately and precisely controlled. The frequency counter used with the gust generator is an integral part of its associated equipment. In this case, the desired frequency corresponds to a specific shaft speed of the gust generator. Thus, by adjusting the

frequency counter to the desired shaft speed, the gust generator is properly set.

2.4.3 Tape and Chart Recorders

To record the output of the amplified strain-gage signals, a Hewlett Packard 4 channel Model 3960 tape recorder was used. This recorder was the primary data collection instrument. The four signals recorded on the tape recorder were the 1/rev pulse, a torsion output signal, chordwise output signal, and a flapping output response signal. At the beginning of each data run, an audio input describing rotor configuration and test conditions was recorded to label that section of the tape. Each recorded section was then played back through a Federal Scientific Corporation Spectrum Analyzer and a plot of the frequency response of the torsion, flapping, and chordwise signals as this test condition was made. This data was then used to compare against theoretical predictions.

In addition to the taped audio signal of each test run, a printed record of each test run was also made using the Honeywell 1508 Visicorder Oscillograph. Utilizing six of the available twelve channels, the signals for the rotor shaft speed, gust generator speed (i.e., frequency), torsional response, chordwise response, and two flapping response signals were recorded. This record served primarily as the back-up data source of the same data which was recorded on the Hewlett Packard tape recorder.

2.4.4 Oscilloscope

Two oscilloscopes were used during the actual test runs. The first scope was marked with a safety circle and served as the primary safety monitoring device. With a chordwise signal input to the x-axis beam and a

flapping signal input to the y-axis beam, the depicted output represented coupled flapping motion. The circle was marked on the scope face such that maximum chordwise motion would be reached at a bending stress of 45 ksi. A flapping limitation was established at $\pm$ 7 deg., or slightly less than the $\pm$ 9 deg. limit established by the rubber flapping stops on the flapping cuff.

A second oscilloscope provided the means to monitor whichever of two output signals was desired. One channel of this oscilloscope was wired to a 9-position channel selection box. This selector box enabled selection of any of the nine output channels from the three blades such that two signals could be either compared or monitored simultaneously. This scope was particularly useful for monitoring transient effects resulting from varying tunnel speeds and varying gust frequencies. Its capability of storing and displaying a signal also allowed for rapid approximate checks against theoretical predictions during actual test runs.

2.4.5 Other

An associated piece of equipment used to analyze data after the completion of test runs was the Federal Scientific Model UA-14 Spectrum Analyzer.

The recorded data was fed to the analyzer from a single channel of the tape recorder for the particular portion of the test sequence under investigation. This signal is placed in storage, Fourier-analyzed, and then presented for examination at an output terminal on a convenient time base, in parallel with the spectrum presentation. The elected option of a plotted output produced an easily discernable frequency record of each channel

(torsion, lead-lag, flap) for each step of the test sequence.

A picture of the instrument control panel in the Wright Brothers Wind Tunnel is shown in Fig. 24.

3. EXPERIMENTAL TEST PROCEDURE

3.1 General Setup and Procedures Prior to Test

3.1.1 Structural Stability and Integrity

Having completed the construction of the model rotor, final preparations for the wind tunnel testing were performed. As outlined in the instrumentation subsection, strain gages were calibrated. Electrical connections from the model hub were rechecked and verified through the slip rings and amplifiers. The rotor shaft alone was rotated at 955 RPM and was checked for balance and alignment. The gust generator rollers were rotated and were checked for frequency/RPM correlation. The model blade tips were each painted a separate distinctive color and the rotor blades were set to 0° collective pitch at the three-quarter chord radius. With the rotor spinning at 400 RPM, an initial stability check of structural integrity of the model design and initial check of the rotor track was performed. The track check was accomplished by using an overhead mounted mirror, canted in such a way that by standing perpendicular to the rotor tip path plane and illuminating the mirror with a strobotac pulsing at three times the rotational speed, the superimposed image of the three blade tips appeared stationary. The only means available for adjusting rotor track on this model was by making small, appropriate collective changes in the pitch setting of the "off-track" blade. This procedure proved quite effective and produced a rotor track where all three blade tip images nearly overlapped. The blade

pitch angle at the 3/4 chord was then increased to 4 deg and finally to 8 deg, which was the pitch angle to be used for the actual test configuration. Structural stability during all of these preliminary tests appeared quite good. The overhead mirror was later removed after the 955 RPM track check and prior to actual testing in order to reduce any possible aerodynamic interference effects with the model rotor. Stability tests were also performed at the rotor rotational speed of 955 RPM with no tunnel velocity.

The next step involved rotating the wind tunnel balance turntable to a shaft angle of 10 deg ($\alpha_s = 10°$) and applying an initial tunnel velocity. The rotor shaft angle was changed from 0° prior to applying tunnel wind in order to avoid any possible stalling of the model rotor. Tunnel velocity was increased to 30 MPH and then to 60 MPH. The rotor response was closely checked at these two speeds, since these two tunnel speeds were to be used for the μ =0.2 and μ =0.4 configurations, respectively. Having again confirmed rotor stability, it was now necessary to determine pressure settings of the gust generator plenum chamber in order that a generated gust would be "seen" and responded to by the rotor.

Preliminary testing revealed that for μ = 0.2 and μ = 0.4 configurations, plenum pressure of 4 psi with gust generator RPM varying from 100 to 500 RPM produced acceptable rotor response. At speeds greater than 500 RPM, the response was very difficult to distinguish primarily because of the downstream gust dissipation at these higher speeds. However, the low frequency gust responses were of greatest interest. Thus, the decision was made to restrict the gust generator speeds to 500 RPM and below for the actual testing. A graph of the gust amplitude for the frequencies and

tunnel speeds used during the model testing is shown in Fig. 25.

3.1.2 Balancing the Rotor

3.1.2.1 Static Balance

A static balance of the rotor system was accomplished in each configuration prior to actually spinning the rotor. For the configuration of one operable blade and two dummy blades, the complete blade assembly of the single blade was weighed and its center-of-gravity located. Based upon these various values of total mass and center-of-gravity locations, weights were added to the two dummy blades to satisfy not only mass considerations, but also the center-of-gravity requirements. The three blades were then attached to the rotor hub and the hub was suspended by means of a plug in the hub center to check the static balance of the assembly. Minor adjustments of the dummy blade weights were then made to complete the rotor static balance.

3.1.2.2 Dynamic Balance

Having completed the static balance, it was now necessary to perform a dynamic balance before each wind tunnel test series. This dynamic balance was accomplished primarily through the use of a General Radio Company Model 1551B accelerometer attached near the hangar bearing of the left mounting trunnion of the wind tunnel balance. The model was spun at operating (testing) RPM with the output of the accelerometer being displayed on an oscilloscope. Again making minor alterations in the locations of the additional weight of each dummy blade, the accelerometer signal could be nearly nulled. In this way, the motion of the shaft, the hangar bearing,

and the trunnion mechanism was minimized. This dynamic balancing eliminated severe model oscillations, reduced the forces exerted on the wind tunnel balance mechanism, and achieved the balance of each model configuration which was so necessary in order to conduct the appropriate wind tunnel test.

Having finished all calibration tests and stability checks on the conditions of the proposed test, it was now possible to proceed to the actual testing and data acquisition.

3.2 Sequence of Actual Testing

3.2.1 General Comments

3.2.1.1 Hovering Configuration

Prior to beginning each actual test, each blade was checked for signal output. With the blade hanging in a vertical position, each strain-gage bridge of that blade was zeroed. These values were recorded and were used later to determine any offset voltage or amplifier drift. The shaft angle was 10 deg ($\alpha_s = 10°$), but a hovering configuration was still achieved since the wind tunnel had no velocity. The rotor was brought up to a rotational speed of 955 RPM (100 rad/sec) and data were recorded. The hovering data for each test configuration were taken at the beginning of each test run.

3.2.1.2 Forward Flight Configuration

With the rotor spinning at 955 RPM and the shaft angle equal to 10 deg, the wind tunnel velocity was now slowly increased to 30 MPH. Rotor response for the $\mu = 0.2$, no gust configuration was then recorded. At this point, the 4 psi gust was added and the test sequence as shown in Table 3,

Column 1, was continued with data recorded at all test settings. Having completed the $\mu = 0.2$ sequence of tests, the tunnel velocity was increased to 60 MPH ($\mu = 0.4$) and the test sequence as outlined in Column 2 of Table 3 was followed. Upon completion of this sequence, the gust generator was turned off and the data for the 60 MPH, no-gust configuration was recorded. Having recorded all necessary data for this portion of the rotor model test sequence, the wind tunnel and rotor model were turned off in that order. It should be noted that emergency switches existed to turn off the rotor model hydraulic pump or Wright Brothers Wind Tunnel if an emergency condition arose during any of the testing. Had the wind tunnel and the rotor been operating, the emergency procedure involved shutting off the wind tunnel before the hydraulic pump, since $\mu = V_{tunnel}/V_{tip}$ and accomplishing emergency shutdown in reverse order would have meant μ would pass through infinity. This would likely produce catastrophic results with regard to the rotor model.

3.2.2 Three-Bladed, Standard Torsion, Undamped

The first rotor test series was begun with the three-bladed, undamped configuration employing standard torsion stiffness. Data were never acquired in this configuration, however, because of a lead-lag resonance which was encountered near 610 RPM. Because of the possibility of exceeding chordwise bending stress limitations of the metal flexure, the test was stopped and the original lead-lag damper shown in Fig. 12 was designed and attached to the model.

3.2.3 Three-Bladed, Standard Torsion, Damped

With the lead-lag dampers now in place, the test series was continued. The dampers functioned extremely well and limited chordwise bending stress of the metal flexures to 10 ksi at the resonance point encountered near 610 RPM. With this problem solved, the rotor speed was increased to 955 RPM. It was now possible to acquire data for this rotor configuration.

3.2.4 Single-Bladed, Standard Torsion, Old Damper, No Tip Weight

The next test involved removing two of the operable blades and replacing them with dummy blades. As mentioned before, the one operable blade configuration was used primarily to eliminate the risk of complete model destruction in the event of some unpredicted rotor instability and to simplify variation of blade CG. At this point in the test series, the redesigned lead-lag damper was still being prepared. Consequently, despite knowing of the large steady-state torsional displacement caused by the original lead-lag damper, it was used on the single operable blade because the lead-lag resonance still existed. Data were acquired for this rotor configuration and served primarily to demonstrate the difference in rotor reaction between the three-bladed rotor versus one-bladed rotor (old dampers) and between the single-bladed configuration of old damper versus new damper cases. Additionally, operation of the single-bladed case was confirmed as no rotor instabilities were evident.

3.2.5 Single-Bladed, Standard Torsion, New Damper, No Tip Weight

Having completed the construction of the redesigned lead-lag damper, it now took the place of the originally designed damper on the model. As expected, the steady-state torsional displacement resulting with this arrangement was far less than the previous steady-state torsional displacement. Data were therefore recorded for this configuration.

3.2.6 Single-Bladed, Standard Torsion, New Damper, Tip Weight Applied, Variable Chordwise Center-of-Gravity

The next portion of the test sequence provided some of the very critical information of the model testing. After securing the tip weight sleeve to the model rotor blade, the tungsten slug was positioned in the sleeve to place the chordwise center-of-gravity at the 25% chord location. In this forward CG location, a blade instability was not expected, but was watched for. The rotor remained very stable so data were recorded.

The tungsten slug was now moved backwards in the tip weight sleeve, moving the chordwise center-of-gravity to the 35% chord location. While a blade instability was more likely in this rearward location, the actual CG shift aft was only 2% from that of the blade without the tip weight assembly. The blade remained stable so data were recorded for this position.

The tungsten slug was finally moved to the most forward location in the sleeve or the 18% chordwise center-of-gravity position. In this configuration, the rotor again appeared to be very stable, so after reconfirming the static and dynamic balance, data were recorded.

3.2.7 Single-Bladed, Soft Torsion, New Damper, Tip Weight Applied, Variable Chordwise Center-of-Gravity

With the completion of the test sequence outlined in the last subsection, the most important and most critical portion of the rotor testing was begun. The metal flexure connecting the rotor blade to the rotor hub was changed from the standard torsion flexure to the soft torsion flexure. The tip weight remained at the 18% chordwise center-of-gravity location. Because of this forward chordwise CG location, no blade instability was suspected, but the rotor was carefully monitored to insure some unforeseen condition could not or did not arise. Again, having confirmed rotor balance and apparent stability, the rotor test sequence was begun and data were acquired.

Next, the tip weight was moved aft to the 25% chordwise center-of-gravity position. The rotor performed extremely well and again appeared quite stable. Data were, therefore, recorded for this configuration.

The final test of the entire model testing sequence was now begun. The tip weight was moved to the 35% chordwise center-of-gravity location. In this configuration, rotor instability was considered likely. However, during preliminary checks and during the balancing procedures for this configuration, the rotor behaved quite normally. Therefore, the rotor was held at the operating RPM and following the normal testing sequence as before, data were recorded. The rotor remained stable throughout this entire testing sequence and showed no indication of imminent instability.

With the conclusion of this final test, the wind tunnel testing phase of the model development was complete.

4. DISCUSSION OF RESULTS

4.1 Experimental Results

The frequency response of blade motions to vertical gusts can be expressed in terms of the three frequency-modulated motions $(\Omega+\omega)$, ω, and $(\Omega-\omega)$, where Ω is the rotational speed of the rotor and ω is the gust frequency. The derivation of these three frequency-modulated motions will be shown in the next section, comparison with theory. Rotor cyclic flapping can be expressed as $(\Omega+\omega)$ and $(\Omega-\omega)$, while collective flapping can be expressed as ω. In the following discussion, these definitions will apply to the flapping motions.

4.1.1 Three Bladed Rotor

For the three bladed rotor at $\mu=0.2$ or the 30 MPH configuration, a cyclic flappling peak for $(\Omega+\omega)$ as shown in Figure 26 appears at $(\omega/\Omega)=0.2$. This is due to the resonance at the flapping natural frequency. The response then decreases as the non-dimensionalized frequency increases, primarily because of the decreasing gust magnitude as shown in Figure 25. The lag motions of Figure 27 also have peaks in the vicinity of $(\omega/\Omega)=0.2$ as do the torsional responses (Figure 28). The apparent flap-lag-torsion coupling in this low speed configuration in the vicinity of $(\omega/\Omega)=0.2$ is evidenced in Figures 26, 27, and 28.

At the higher tunnel speed of 60 MPH, the cyclic flapping response is nearly the same as for 30 MPH; however, the peak amplitude of the $(\Omega+\omega)$ response has decreased by 11% (Figure 29). This is due to the gust gradient decreasing at the higher speed. The lag response (Figure 30) maintained nearly the same response motions and magnitudes as Figure 27,

while the torsional motions (Figure 31) seem to have become somewhat independent of any coupling and do not respond as much at the flapping natural frequency.

4.1.2 Center-of-Gravity Shift with Changes in Torsional Stiffness

The flapping response reductions due to the center-of-gravity shifts between the soft and standard flexures in the 30 MPH configuration as shown in Figures 32 and 35 are not obvious. However, it seems that torsional motion has increased in the case of the soft flexure (Figure 33). The apparent lack of flapping motion reduction is because the aerodynamic forces due to the torsional motion are not enough to reduce the flapping motion. As shown in Figures 34 and 37, the lag motion is quite consistent for all center-of-gravity positions for both the soft and standard flexure configurations.

In the 60 MPH configuration, the reduction in flapping response is quite clear. When the standard torsion flexure is used, reduction of $(\Omega+\omega)$ flapping motion is qualitatively observed in Figure 38 and is due to the center-of-gravity shift forward from $35\%\bar{c}$ to $18\%\bar{c}$. Figure 39 shows that the torsional motion is much more significant at the most forward and most aft CG locations, while the lag motion depicted in Figure 40 essentially shows no change from Figure 37. With the soft torsion flexure response shown in Figure 41, however, significant reductions of 25% and 58% can be seen in the $(\Omega+\omega)$ flapping response at $(\omega/\Omega)=0.2$ as the CG location moves from $35\%\bar{c}$ to $25\%\bar{c}$ and from $35\%\bar{c}$ to $18\%\bar{c}$ respectively. In collective flapping, similar reductions are obtained; however, the $(\Omega-\omega)$ response does not show a clear picture. At $(\omega/\Omega)=0.1$ and $(\omega/\Omega)=0.5$, the

reduction mechanism created by the chordwise CG shift apparently is not working. The gust response reduction is more obvious at 60 MPH with the soft torsion flexure because the large torsional motion produced by the soft torsion flexure produces more aerodynamic forces due to the increased advance ratio. Chordwise motions are again very low (Figure 43) and present no significant changes in response between the standard and soft flexure.

An interesting phenomenon is present in the torsional motion response for the higher advance ratio configurations of both the soft and standard flexures. As the chordwise center-of-gravity position is moved aft from 18%$\bar{c}$ to 25%$\bar{c}$, a reduction in response for $(\Omega+\omega)$, ω, and $(\Omega-\omega)$ occurs for both flexure stiffnesses. These motions are shown in Figures 39 and 42. The $(\Omega+\omega)$, ω, and $(\Omega-\omega)$ responses of the 25%$\bar{c}$ location all display the same general motion, that being a slow, steady decrease as (ω/Ω) increases. However, as the chordwise center-of-gravity location is moved further aft to the 35%$\bar{c}$ position, an increased response in all three frequency-modulated motions is observed. This larger response over the entire non-dimensionalized range would indicate that some point of minimal torsional motion with reference to chordwise center-of-gravity location had been reached and passed. Thus, while it might appear that chordwise center-of-gravity shifts could be used to minimize the torsional response motion, the chordwise center-of-gravity position so determined may not be the optimal overall location in view of the desired objective of reducing blade flapping motion.

4.1.3 System Stability, Resonances, and Thrust Measurement

As mentioned previously, the model rotor performed extremely well with regard to stability in all configurations tested. While there was some concern that blade flutter would occur in the 35%$\bar{c}$ CG configuration with the torsionally soft flexure in place, this flutter never developed nor showed any signs of developing. The only system resonance encountered was that near 610 RPM in chordwise motion in the undamped three bladed configuration. It was therefore necessary to design and attach a lead-lag damper. After this damper system was attached to the model there was no further difficulty with the lead-lag resonance point previously encountered.

Attempts to measure the model rotor thrust were unsuccessful. The model balance in the Wright Brothers Wind Tunnel was designed and built to measure side force, and with the model rotor orientation while mounted on the balance in the tunnel, it was felt that this side force measurement could be recorded as the experimental thrust force value of the rotor. However, electrical problems existed in the measuring gages on the wind tunnel balance. After attempting repair of these strain gages, it was determined that any further time spent on this effort would delay the actual model testing program. Thus, the thrust of the model rotor was never measured experimentally. Theoretically the thrust of the rotor was determined to be:

$$T = C_T \rho A (\Omega R)^2$$

$$T = (.006)(.00238)\left[(\pi)\left(\frac{28.65}{12}\right)^2\right]\left[(1.00)\left(\frac{28.65}{12}\right)\right]^2$$

$$T = 14.57 \text{ lb}$$

where C_T = thrust coefficient

ρ = air density

A = disc area

(ΩR) = rotational speed times rotor radius

4.2 Comparison with Theory

4.2.1 General

As stated in Subsection 4.1, the frequency response of blade motion to a vertical gust is explained in terms of three frequency-modulated motions of $(\Omega+\omega)$, ω, and $(\Omega-\omega)$, where Ω is the rotational speed and ω is the gust frequency. These responses can also be explained by the developed theory and through the flapping equation of Reference 17:

$$\ddot{\beta} + (\frac{\gamma}{8} + \mu \frac{\gamma}{6} \sin\psi)\dot{\beta} + \{(\frac{\omega_\beta}{\Omega})^2 + \mu \frac{\gamma}{6} \cos\psi + \mu^2 \frac{\gamma}{8} \sin(2\psi)\} \beta =$$

$$\frac{\gamma}{6} \bar{\omega}_G + \mu \frac{\gamma}{4} \bar{\omega}_G \sin\psi \qquad (A)$$

where

γ : Locke Number

μ : advance ratio

ω_β: Natural Frequency

$\bar{\omega}_G$: gust velocity

ψ : Ωt azimuth

and

$$\bar{\omega}_G = \omega_G \sin\omega t - \frac{\gamma}{8} \omega_G (\frac{\omega}{\Omega}) \frac{1}{\mu} \cos\omega t \cos\Omega t \qquad (B)$$

The first term in Equation B shows a uniform component of the gust velocity over the rotor disc and the second term the nonuniformity of the gust velocity. Substituting Equation B into the right-hand side of Equation A yields:

$$\frac{\gamma}{6}\,\omega_G \sin\omega t + \frac{1}{2}\{\mu\,\frac{\gamma}{4} + \frac{\gamma}{8}\,\frac{1}{\mu}\,(\frac{\omega}{\Omega})\}\cos(\Omega+\omega)t$$

$$+ \frac{1}{2}\{\mu\,\frac{\gamma}{4} - \frac{\gamma}{8}\,\frac{1}{\mu}\,(\frac{\omega}{\Omega})\}\cos(\Omega-\omega)t + \text{higher order terms}$$

Therefore, due to a vertical gust with frequency ω, the flapping motions ω, $(\Omega+\omega)$, and $(\Omega-\omega)$ will be excited.

4.2.2 Three Bladed Rotor

The three bladed rotor case provided basic information regarding the overall response of the rotor model to a vertical gust. Because there was neither a change in torsional stiffness nor chordwise center-of-gravity in this configuration, no specific conclusions could be drawn from the rotor response with regards to the objectives of the test program. Consequently, only the theoretically predicted flapping motions have been included to compare with the experimental results.

Experimental flapping responses at 30 MPH for $(\Omega+\omega)$, ω, and $(\Omega-\omega)$ were all within 15% of the predicted values (Figure 26). In general, the predicted results displayed a slightly greater response to the mid-frequency excitations than was found in the experimental responses. This was particularly true for the $(\Omega-\omega)$ and ω motions. The predicted $(\Omega+\omega)$ motion, however, was very nearly attained by the experimental result with it peaking at a non-dimensionalized frequency of $(\omega/\Omega)=0.2$ and differing only slightly in magnitude.

The predicted flapping responses for the 60 MPH configuration (Figure 29) were more closely attained by the wind tunnel model than in the 30 MPH case. Only the $(\Omega-\omega)$ test response showed a difference in magnitude from that predicted. This predicted response also exhibited a characteristic of the lower tunnel speed case, that being a significant response at at the midrange non-dimensionalized frequency. In this case, the response was a significant decrease at the midrange frequencies. However, based upon the good correlation between predicted flapping motion and observed flapping motion in both the 30 MPH and 60 MPH cases, it was concluded the experimental model provided a valid representation for the desired tests. Therefore, the single bladed configuration involving torsional stiffness variations and chordwise center-of-gravity changes could now be tested.

4.2.3 Center-of-Gravity Shift with Changes in Torsional Stiffness

While the initial wind tunnel tests dealt with the gust response of the three bladed rotor model, the most important portion of the experiment involved the single-operable, two-dummy blade configuration and its testing. The tests of this configuration provided the mose useful information. The comparison of the theoretical rotor responses with those responses actually recorded from the wind tunnel model will now be discussed.

4.2.3.1 30 MPH Configuration

An objective of the test program was to evaluate the effectiveness of torsional stiffness variation in conjunction with chordwise center-of-gravity shifts in alleviating the gust response of a hingeless rotor. Initial theoretical predictions showed that at 30 MPH (μ=0.2), a change in torsional stiffness would produce only small changes in blade flap, torsion, and lag

motion, with these changes being most prevalent in the soft flexure configuration. As described in the experimental results, Subsection 4.1.2, these earlier predictions for the 30 MPH configurations proved correct. Therefore, to avoid repeating similar results, only the theoretical predictions for the soft torsion flexure with a 25% chordwise center-of-gravity location will be compared to the experimental results for this low speed configuration.

The theoretical predictions for flap, torsion, and lag motions of the soft flexure, 30 MPH case, are shown in Figures 44, 45, and 46 respectively. These predictions come very close to forecasting the actual responses achieved from the wind tunnel model. Regarding rotor cyclic flapping, the predicted $(\Omega+\omega)$ response (Figure 44) displayed a 25% lesser excitation at the flapping natural frequency than that achieved by the wind tunnel model (Figure 32). The same was true for the $(\Omega-\omega)$ response, as the predicted lower frequency response was smaller than that achieved by the model. The ω response showed good agreement in both magnitude and motion between the theoretical prediction and the experimental observation.

The predictions for the $(\Omega+\omega)$ and ω responses of torsional motion (Figure 45) were very accurate with regards to results achieved (Figure 33). Only in the $(\Omega-\omega)$ response was the predicted result lower in magnitude than that achieved. Again, as with the difference in flapping response, these lower predicted values were at the lower non-dimensionalized frequencies.

The predicted lag motions (Figure 46) also proved accurate for the $(\Omega+\omega)$ and ω responses when compared to the experimental results (Figure 34). Only in the $(\Omega-\omega)$ was there a difference between predicted and observed

results. Observed results displayed a slowly increasing then decreasing motion as the non-dimensionalized frequency increased, but with no extreme peaking involved. Theoretical results displayed an increasing response, peaking a higher non-dimensionalized frequency in the vicinity of the lag resonance. It is clear why this higher response in the vicinity of the lag resonance was not seen by the wind tunnel model.

4.2.3.2 60 MPH Configuration

As with the 30 MPH configuration, the theoretically predicted 25% chordwise center-of-gravity responses for the soft flexure have been plotted to use as a comparison with the experimentally determined results. As has been shown, chordwise center-of-gravity shifts for the standard torsion flexure produce flapping reductions, but these are more of a qualitative rather than quantitative nature (Figure 38). Overall agreement between theoretical predictions and experimentally obtained results for the soft flexure is quite good, particularly in the important parameters of torsion and flapping. Some discrepancies exist between the predicted and observed lag motion.

Predicted flapping motions are shown in Figure 47. While there is good agreement regarding the tendencies for the $(\Omega+\omega)$ and $(\Omega-\omega)$ cyclic flapping responses, the experimental magnitudes (Figure 41) are not in complete agreement with those predicted. Additionally, the predicted ω motion displays a tendency to remain somewhat constant, while the observed ω motion exhibits more of a tendency to follow the gust characteristic of decreasing in magnitude as the non-dimensionalized frequency increases (Figure 25).

The predicted torsional responses (Figure 48) are very close approximations for the experimental results (Figure 42). These torsional predictions provided the best correlation between theory and experiment for the entire test sequence.

Finally, the lag responses for the soft flexure are shown in Figure 49. The predicted $(\Omega+\omega)$ tendency is verified by the experiemental results, although a difference in magnitude does exist. However, the ω and $(\Omega-\omega)$ responses do display discrepancies between the predicted and observed results. Theory predicts a larger excitation for both of these motions, particularly in the vicinity of the lag resonance $(\omega/\Omega)=0.4$. However, as was also the case with the experimental lag data in the 30 MPH configuration, the model does not exhibit this excitation response at the higher non-dimensionalized frequency. It is still not clear why this discrepancy exists between the theoretical predictions and the experimental results.

5. CONCLUSIONS AND RECOMMENDATIONS

5.1 Conclusions

The wind tunnel testing was designed to examine the theory regarding the response of hingeless rotors to vertical gusts and to validate the effectiveness of blade center-of-gravity shifts as a gust alleviation method.

Based upon the experimental results of the wind tunnel tests, the following conclusions may be stated:

(a) Chordwise center-of-gravity shifts are a simple and effective means of alleviating hingeless rotor gust response. In the wind tunnel model utilizing a stiff torsional flexure, $\mu=0.4$, and employing a 17% center of gravity shift from a most aft to

a most forward configuration, a 32% decrease in collective flapping is achieved. In the case of a torsionally soft flexure, μ=0.2, and a 7% center-of-gravity shift towards the leading edge, a 2-3% decrease in collective flapping is achieved. At a higher advanced ratio of μ=0.4, the same torsionally soft flexure yields a 25% reduction in the collective flapping for the same 7% forward center-of-gravity shift. Results of shifting the CG from the most aft to the most forward location (17% overall) yields a 58% reduction in collective flapping.

(b) Reduced torsional stiffness produces reduction in the flapping response. While more of a qualitative reduction at the lower advance ratio, the overall flapping motion reduction is more discernable at the higher advance ratio. This is particularly true in the more forward center-of-gravity configurations.

5.2 Recommendations

Recommendations regarding the continued refinement of the proposed theory and its wind tunnel model can be classified into two activities. One activity would involve the construction of a full scale rotor and the testing of that system to further validate the gust alleviation mechanism by altering the chordwise center-of-gravity location in conjunction with varying the torsional stiffness. Successful tests of a full scale rotor would add practical credibility to the developed theory. A second activity would involve the continuation of a wind tunnel test program involving the present model. This program could perfect the techniques already validated

and further establish this scheme as a means of alleviating the rotor response to gusts. Some of the specific changes and improvements that would be applicable to the model if time and money permitted might include:

(a) Addition of cyclic pitch. This could be accomplished most easily by incorporating into the model design an electronic as opposed to mechanical swashplate, a cyclic servo motor for each blade, and the necessary feathering bearings for this motion in the rotor hub.

(b) With the addition of cyclic pitch, a feedback controller could be added. The controller would receive the output signal generated by the strain gages and after interpretation, apply the necessary control input to help alleviate the effect of the gust. This active control system would then supplement the passive system of center-of-gravity shift and together they would serve as the means of alleviating the rotor response to a vertical gust.

(c) Design, construct, and test blades that would incorporate into their blade sections the capability of varying the chordwise CG location. This could be accomplished by constructing hollow blades with specially designed compartments. By positioning a weight in the appropriate compartment in the blade, the desired center-of-gravity shift could be achieved. This feature would eliminate any external parts being attached to the blade. Additionally, this improved design would eliminate the need to construct a special counterweight sleeve, eliminate the

drilled holes in the model blade for attaching the tip weight sleeve, and provide a much cleaner and more accurate aeroelastic model.

(d) Improve the flapping flexure design by placing more slack in the lead-in wires and by using a newly developed low-temperature soldering technique. This would eliminate some of the electrical problems associated with the model testing.

REFERENCES

1. Yasue, Masahiro, "Gust Response and Its Alleviation for a Hingeless Helicopter Rotor in Cruising Flight". Massachusetts Institute of Technology, Aeroelastic and Structures Research Laboratory, ASRL TR 189-1, January 1977.

2. Lauten, T. and Martin, D.J., "Measurement of Structural Influence Coefficients". AGARD Manual on Aeroelasticity, Volume IV, Chapter 1, October 1961.

3. Bisplinghoff, Raymond L., Ashley, Holt, and Halfman, Robert L., Aeroelasticity. Addison-Wesley Publishing Company, Reading, Massachusetts, 1955.

4. Rauscher, M., Aeronautical Dynamics. John Wiley and Sons, New York, 1953.

5. Zvara, John, "The Aeroelastic Stability of Helicopter Rotors in Hovering Flight". Massachusetts Institute of Technology, Aeroelastic and Structures Research Laboratory, ASRL TR 61-1, September 1956.

6. Ham, Norman D., Bauer, Paul H., and Lawrence, Thomas L., "Wind Tunnel Generation of Sinusoidal Lateral and Longitudinal Gusts by Circulation Control of Twin Parallel Airfoils", Massachusetts Institute of Technology, Aeroelastic and Structures Research Laboratory, ASRL TR 174-3, and also NASA CR 137547, August 1974.

7. Gayman, W.H., "Investigation of Effect of Varying Tip Weight". Journal of Aeronautical Science, May 1952.

8. Peery, D.J., Aircraft Structures. McGraw Hill, New York, 1950.

9. "Proprotor Development". Journal of the American Helicopter Society, Vol. 17, No. 1, January 1972, pp 6-18.

10. Wasserman, L.S. and Mybrytow, W.J., "Model Construction". AGARD-CP-578, January 1961, Chapter 7.

11. Reissner, E. and Stein, M., "Torsional and Transverse Bending of Cantilevered Beams and Plates". NACA TN 2369, June 1951.

12. Teichman, F.K., Airplane Design Manual. Pitman Company, New York, 1939.

13. Cook, N.A. and Rabinowitz, E., Physical Measurement and Analysis. Addison Wesley Publishing Company, Reading, Massachusetts, 1963.

14. Silveria, Milton A., Maglien, Domenic J., and Brroks, George W., "Results of an Experimental Investigation of Small Viscous Dampers". Langley Aeronautical Laboratory, NACA TN 4257, June 1958.

15. Sissingh, G.I., "Response Characteristics of the Gyro Controlled Lockheed Rotor System". Lockheed Aircraft Corporation Report LR 20581, date unknown.

16. Hohenemser, K.H., "Hingeless Rotorcraft Flight Dynamics". AGARD-CP-197, September 1974.

17. Ham, Norman D., "Helicopter Blade Flutter". AGARD-R-607, January 1973.

TABLE 1

DESCRIPTION OF THE ROTOR BLADE

USED IN THE WIND TUNNEL TEST

Number of Blades	3
Radius, R	2.375 ft
Chord, C	2 in
Locke number, γ (standard torsion)	2.65
Solidity, σ	0.0670
Collective pitch, θ_0	8 deg
Shaft tilt angle in cruising flight, α_s	10 deg forward
Lift-curve slope, a	5.7
Drag coefficient, Cd_0	0.012
Rotational speed, Ω	100 rad/sec (955 RPM)
Built-in blade angle of twist, θ_{TW}	8 deg (linear)
Elastic Axis	33% chord
Aerodynamic center	25% chord
Precone	0 deg
Droop	0 deg
Torque offset	0 in
Control linkage flexibility	rigid
Basic natural frequencies	
Lag	0.723/rev
Flap	1.142/rev
Torsion	6.12/rev (standard)
	3.66/rev (soft)

TABLE 2

CHORDWISE CENTER-OF-GRAVITY POSITIONS

CHORDWISE CG POSITION	18%	20%	25%	30%	35%
WEIGHT	2.120	1.661	0.530	0.600	1.730
LOCATION	INCHES FORWARD OF THE LEADING EDGE	INCHES FORWARD OF THE LEADING EDGE	INCHES FORWARD OF THE LEADING EDGE	INCHES AFT OF THE LEADING EDGE	INCHES AFT OF THE LEADING EDGE

TABLE 3

TEST SEQUENCE

HOVERING CONFIGURATION V_{TUNNEL} = 0 NO GUST					
FORWARD FLIGHT CONFIGURATION V_{TUNNEL} = 30 MPH NO GUST					
FORWARD FLIGHT CONFIGURATION					
V_{TUNNEL} = 30 MPH			V_{TUNNEL} = 60 MPH		
GUST GENERATOR			GUST GENERATOR		
FREQ	RPM	PRESSURE	FREQ	RPM	PRESSURE
1.67	100	4 PSI	1.67	100	4 PSI
2.50	150	4 PSI	2.50	150	4 PSI
3.33	200	4 PSI	3.33	200	4 PSI
4.17	250	4 PSI	4.17	250	4 PSI
5.00	300	4 PSI	5.00	300	4 PSI
6.67	400	4 PSI	6.67	400	4 PSI
8.33	500	4 PSI	8.33	500	4 PSI
FORWARD FLIGHT CONFIGURATION V_{TUNNEL} = 60 MPH NO GUST					

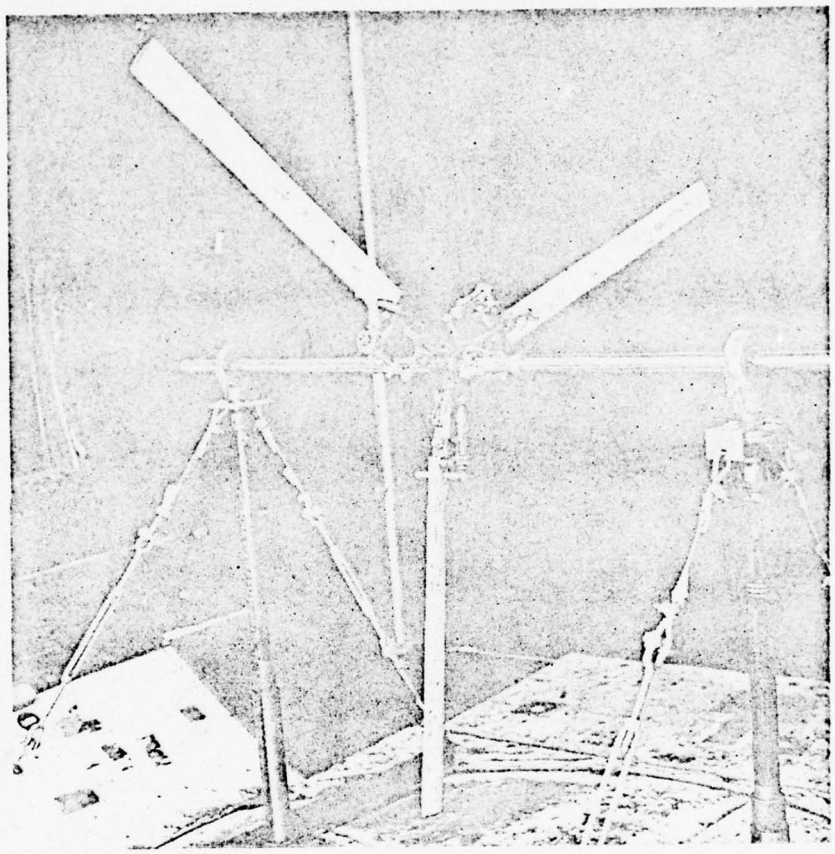

FIGURE 1 THREE BLADED ROTOR

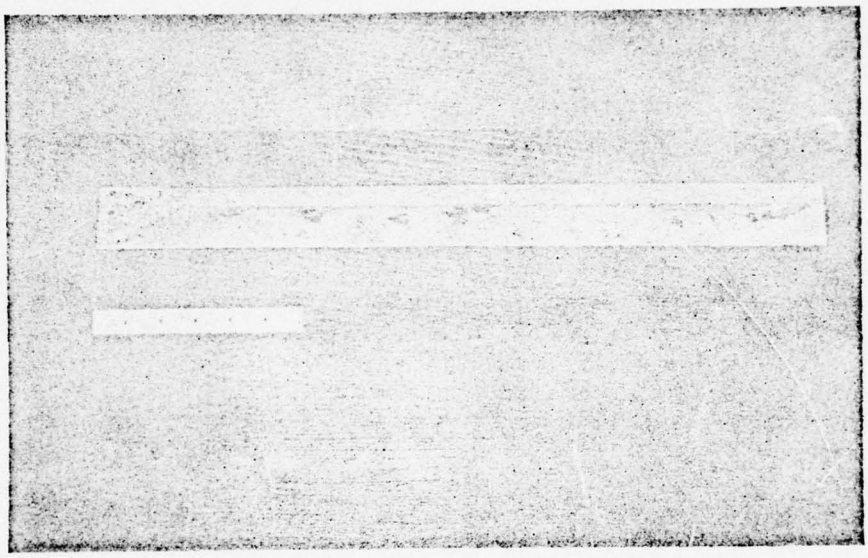

FIGURE 2 MODEL ROTOR BLADE

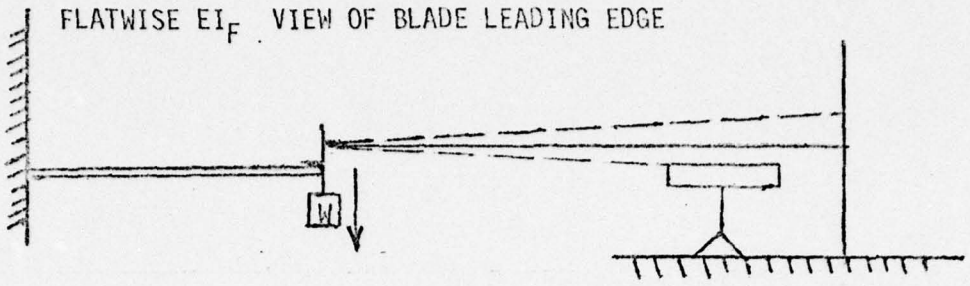

FIGURE 3 EI_F MEASUREMENT SCHEMATIC

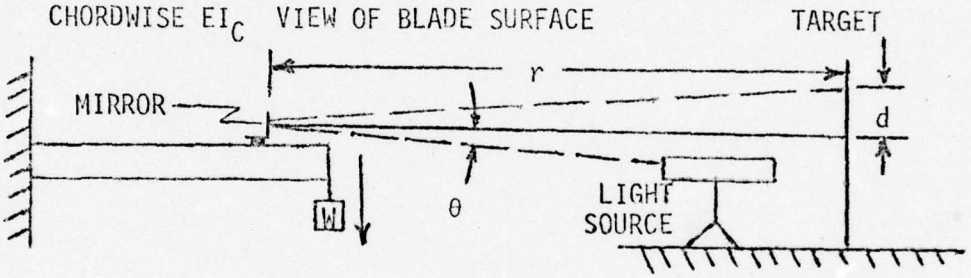

FIGURE 4 EI_C MEASUREMENT SCHEMATIC

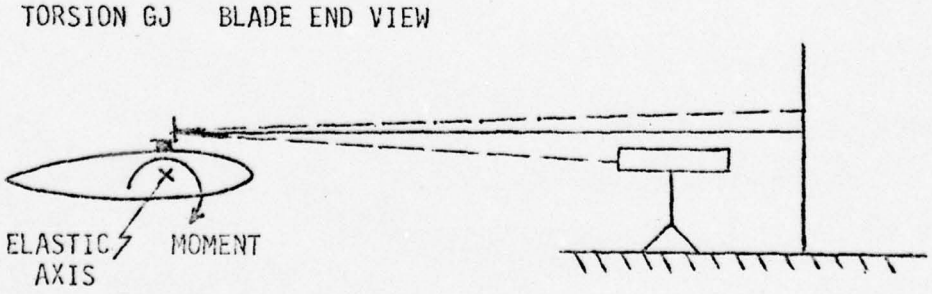

FIGURE 5 GJ MEASUREMENT SCHEMATIC

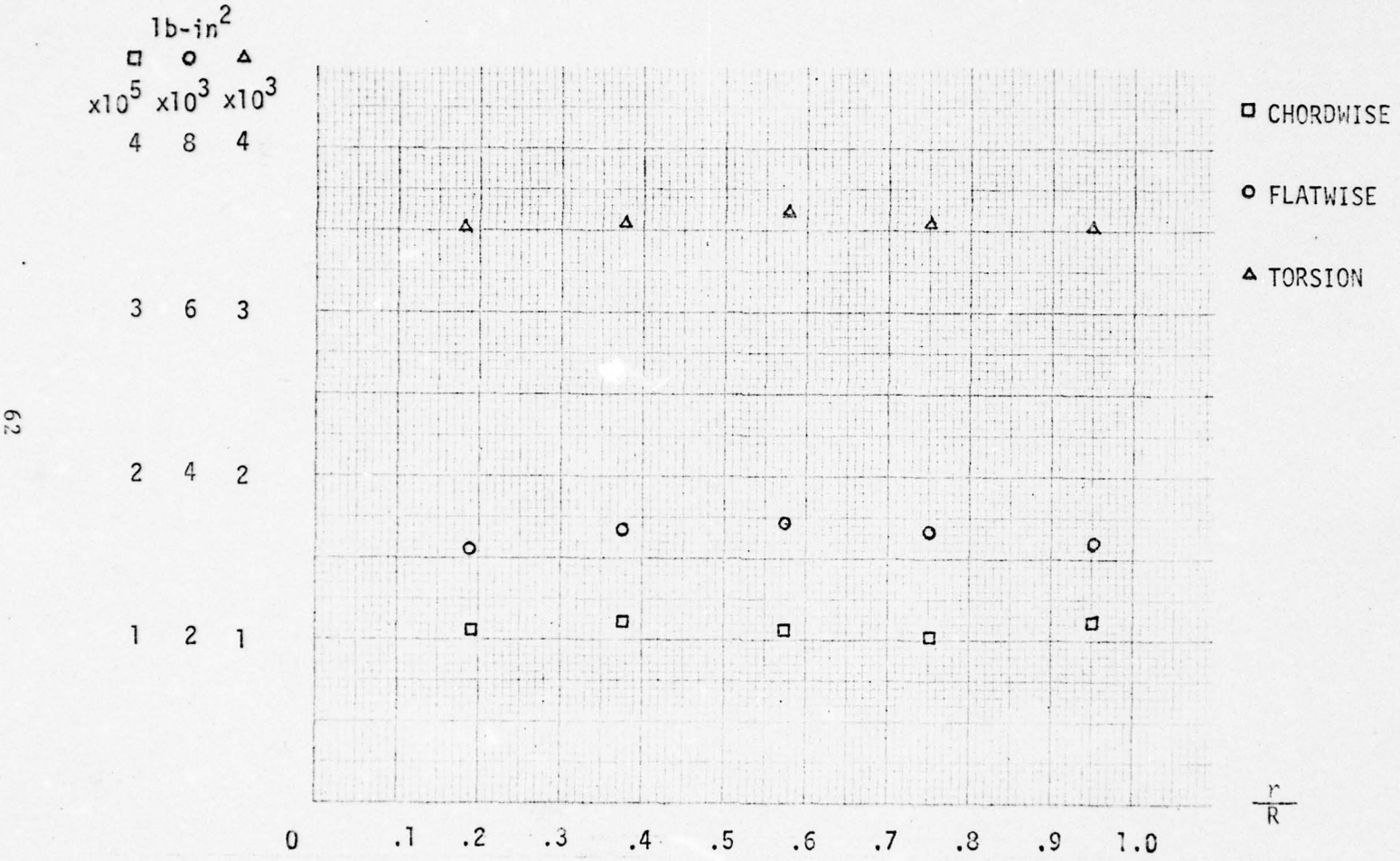

FIGURE 6 MEASURED BLADE STIFFNESSES

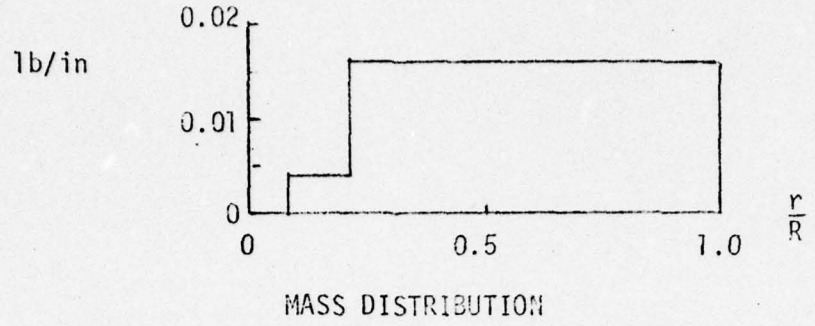

MASS DISTRIBUTION

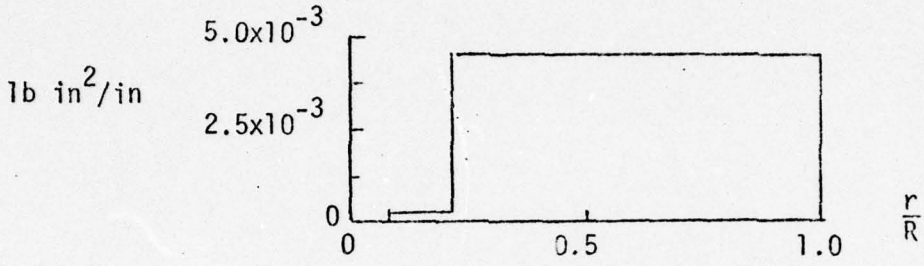

CROSS-SECTIONAL MOMENT OF INERTIA

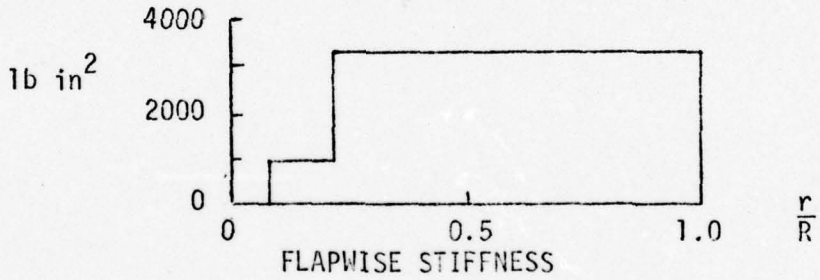

FLAPWISE STIFFNESS

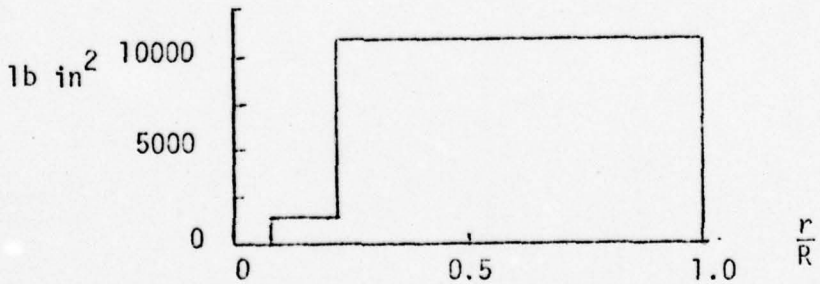

CHORDWISE STIFFNESS

FIGURE 7 FLEXURE AND BLADE PARAMETERS
(0.0R TO 0.079R IS RIGID)

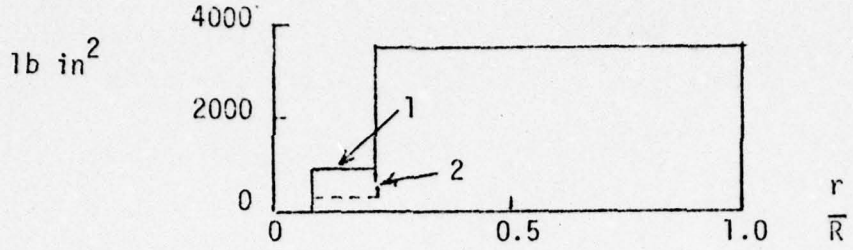

TORSIONAL RIGIDITY

1 STANDARD TORSIONAL STIFFNESS

2 SOFT TORSIONAL STIFFNESS

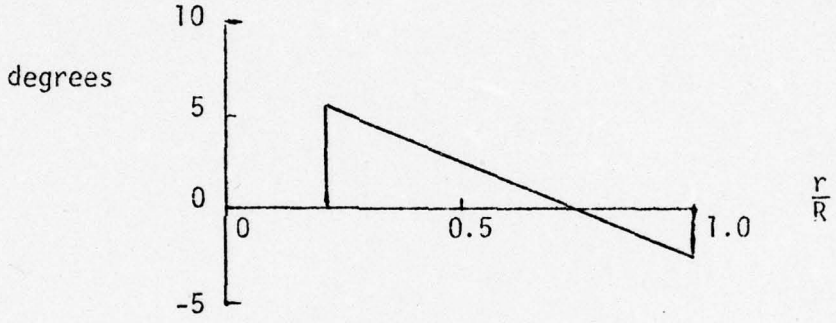

ANGLE OF TWIST

FIGURE 7 FLEXURE AND BLADE PARAMETERS CONCLUDED

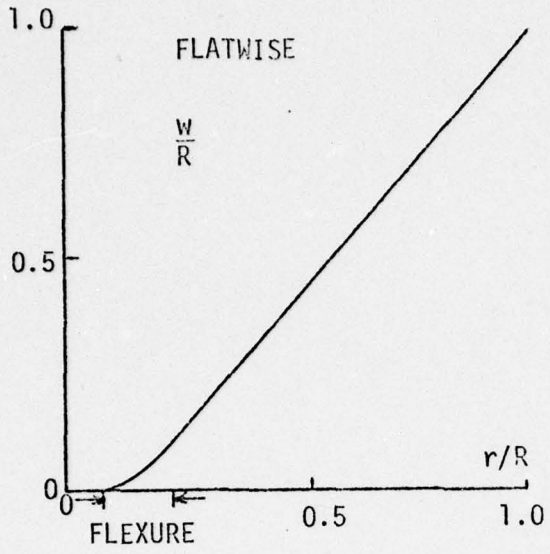

NATURAL FREQUENCY
1.14/ REV

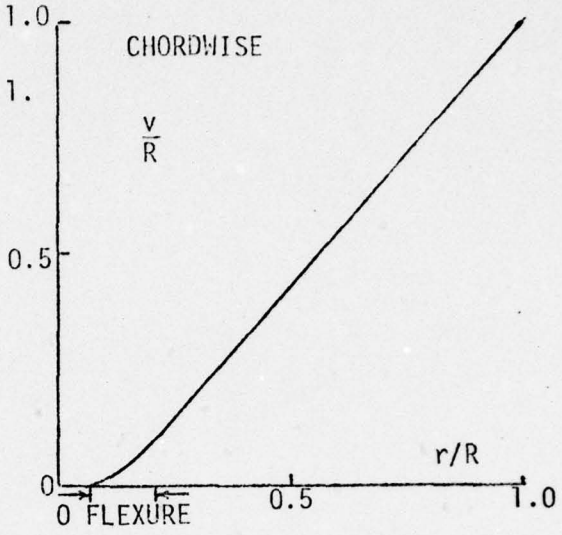

NATURAL FREQUENCY
0.72/ REV

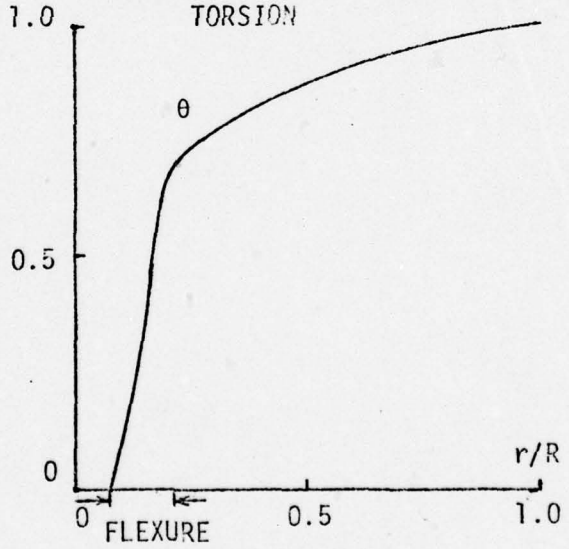

NATURAL FREQUENCY
6.12/ REV

FIGURE 8 RECTANGULAR FLEXURE MODE SHAPES

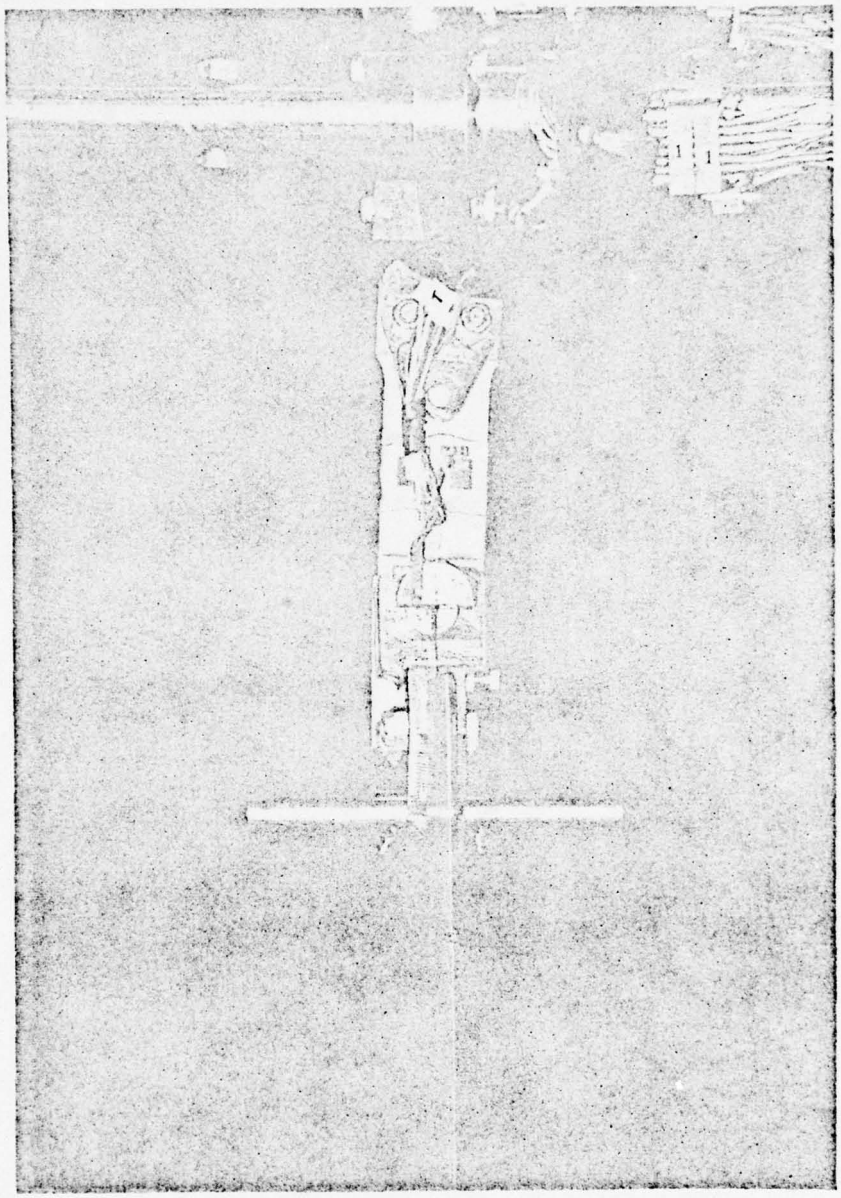

FIGURE 9 METAL FLEXURE, FLAPPING CUFF, AND BLADE COUNTERWEIGHTS

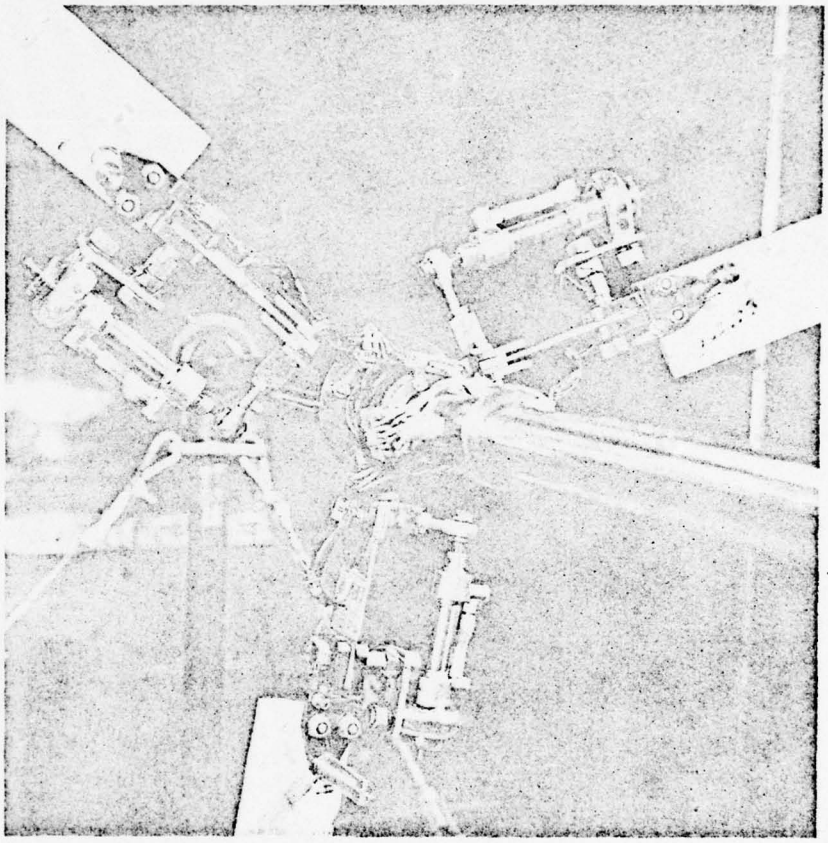

FIGURE 10 ROTOR HUB WITH THREE BLADES MOUNTED

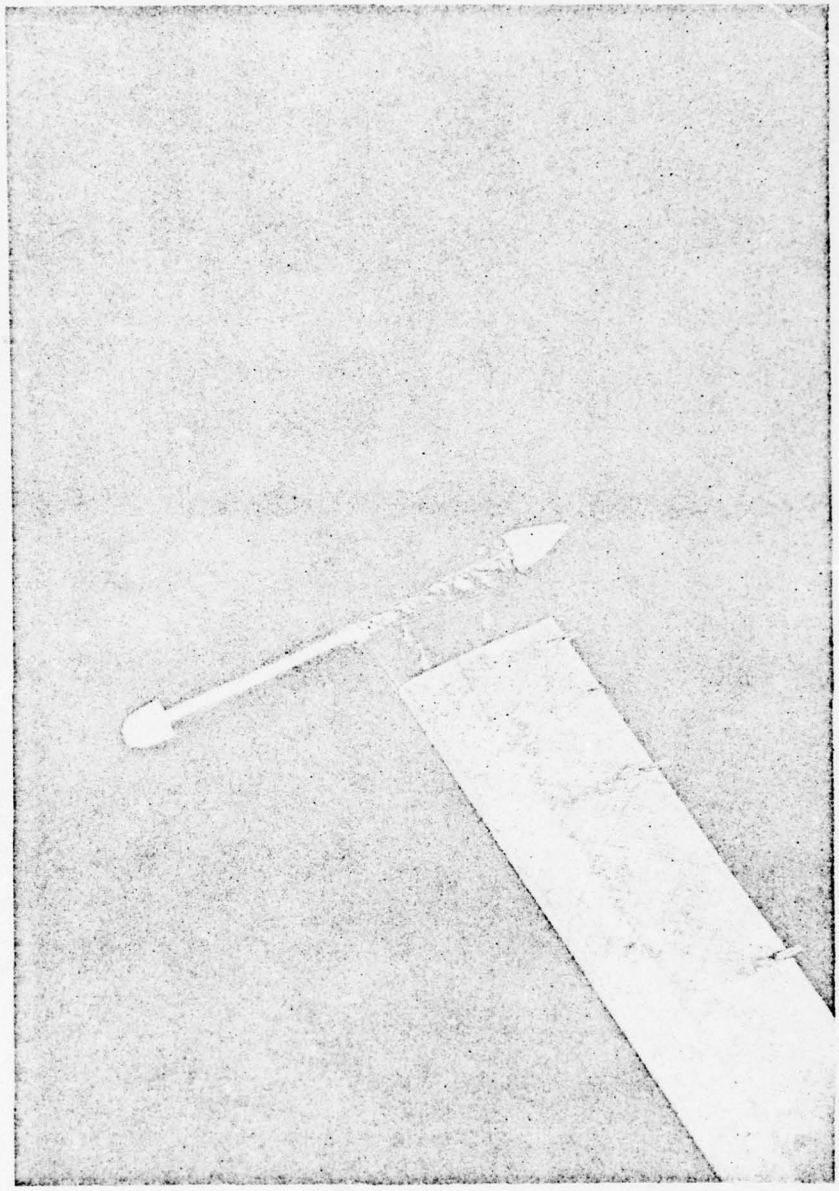

FIGURE 11 BLADE WITH TIP WEIGHT ASSEMBLY

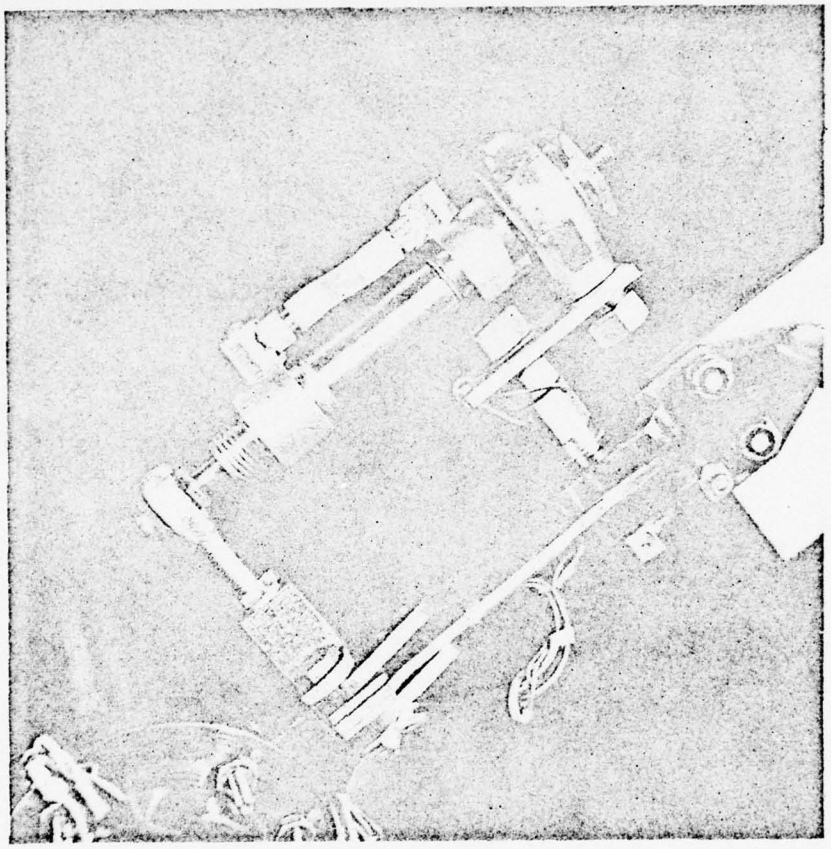

FIGURE 12 ORIGINAL LEAD-LAG DAMPER

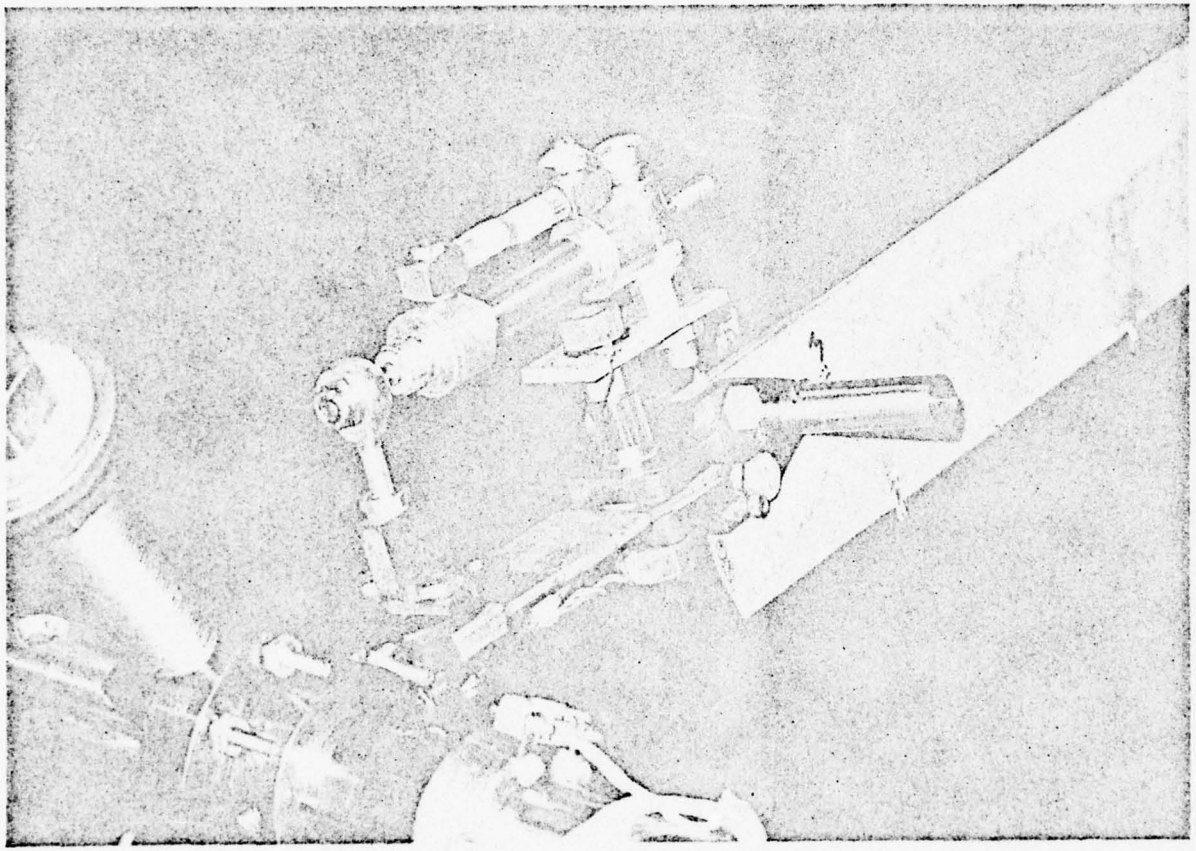

FIGURE 13 REDESIGNED LEAD-LAG DAMPER

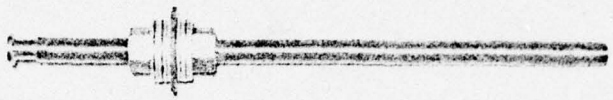

FIGURE 14 DUMMY BLADE AND BALANCING WEIGHT

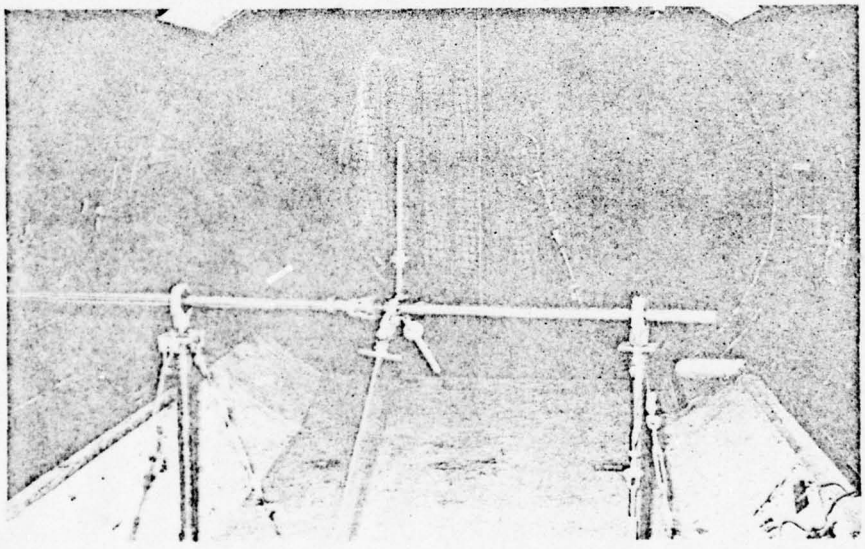

FIGURE 15 MODEL INSTALLATION, DOWNSTREAM VIEW

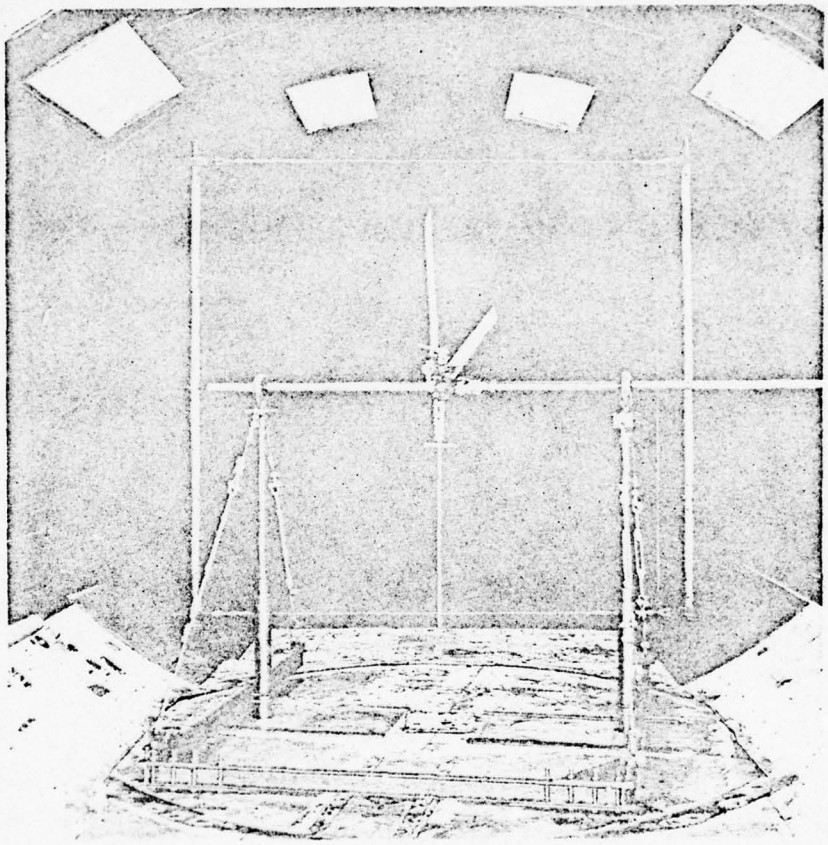

FIGURE 16 MODEL INSTALLATION, UPSTREAM VIEW

FIGURE 17 SPLINED BALL SHAFT COUPLING

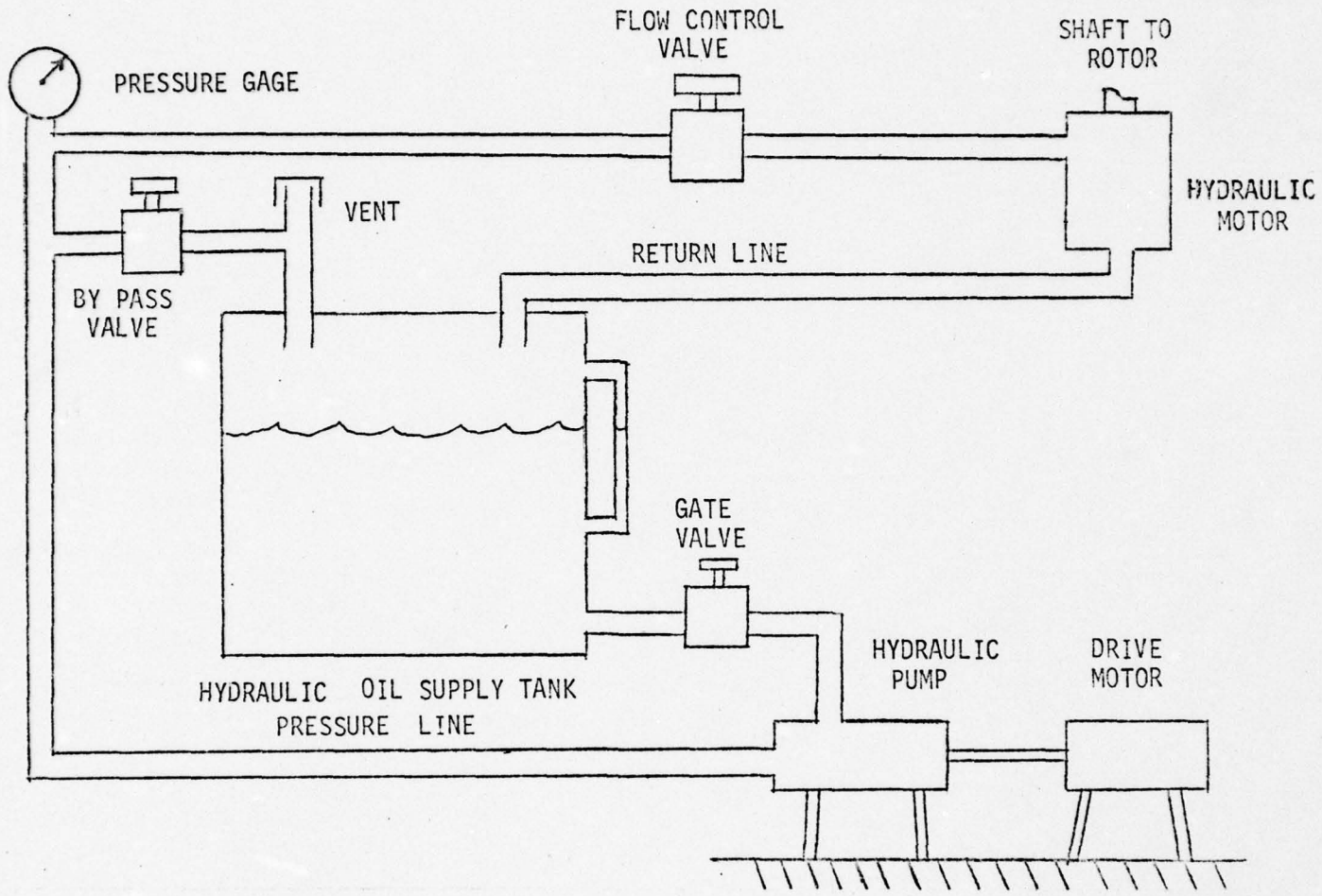

FIGURE 18 HYDRAULIC SYSTEM SCHEMATIC

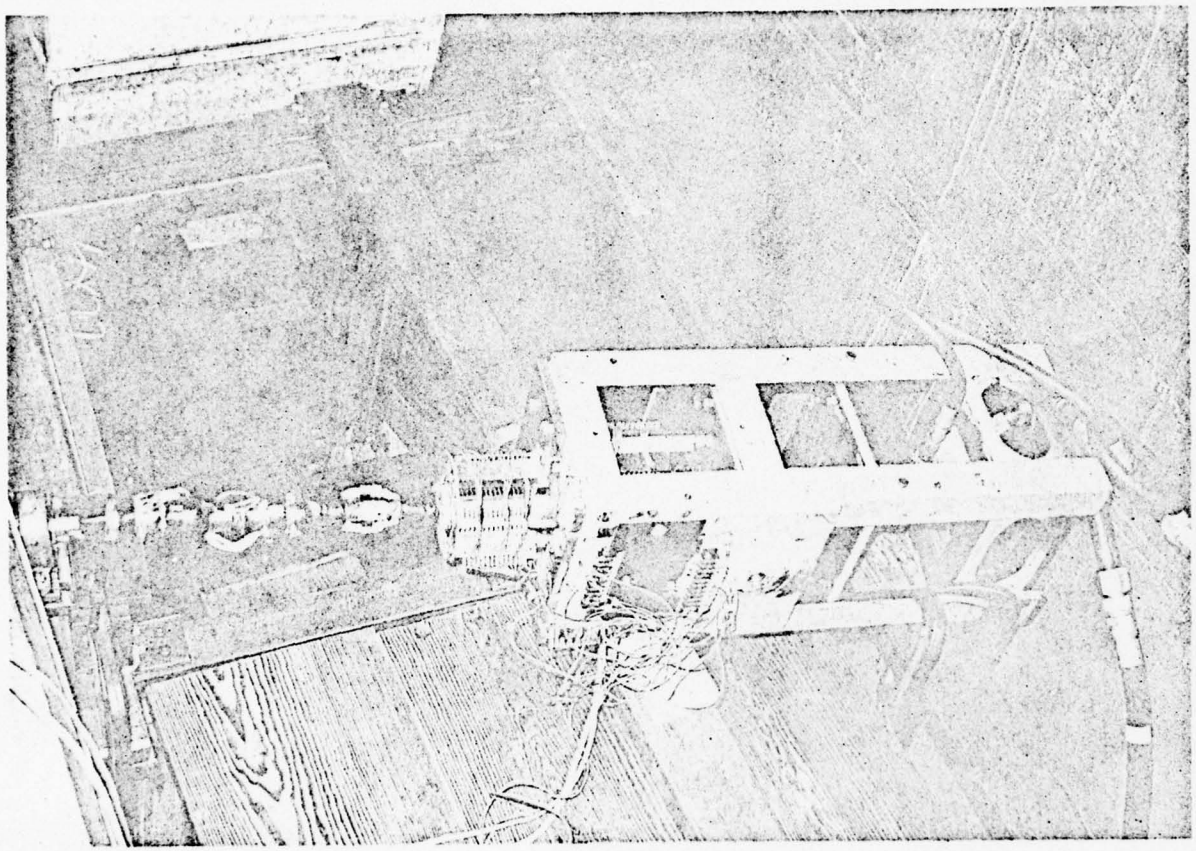

FIGURE 19 HYDRAULIC MOTOR AND SLIP RING ASSEMBLY

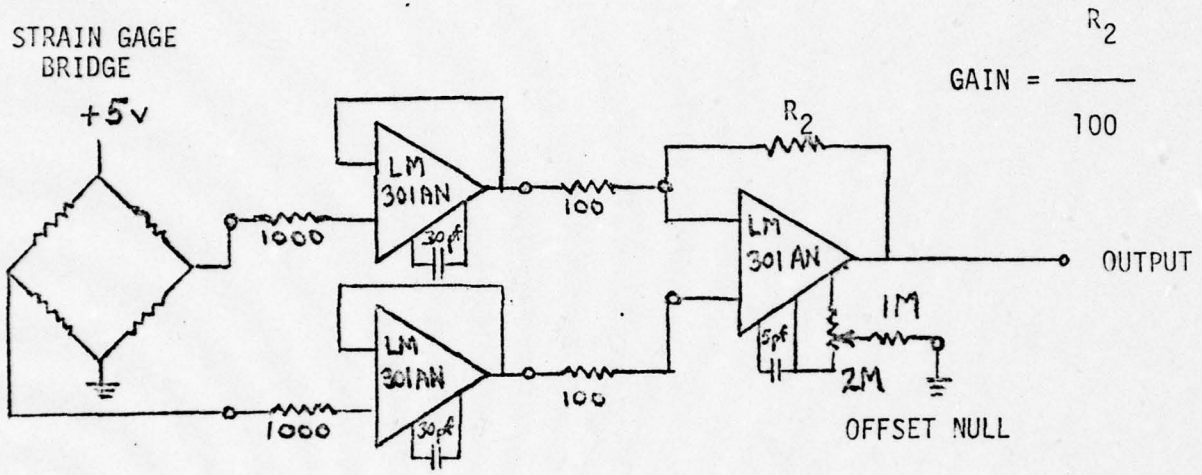

FIGURE 20 STRAIN GAGE AMPLIFIER SCHEMATIC

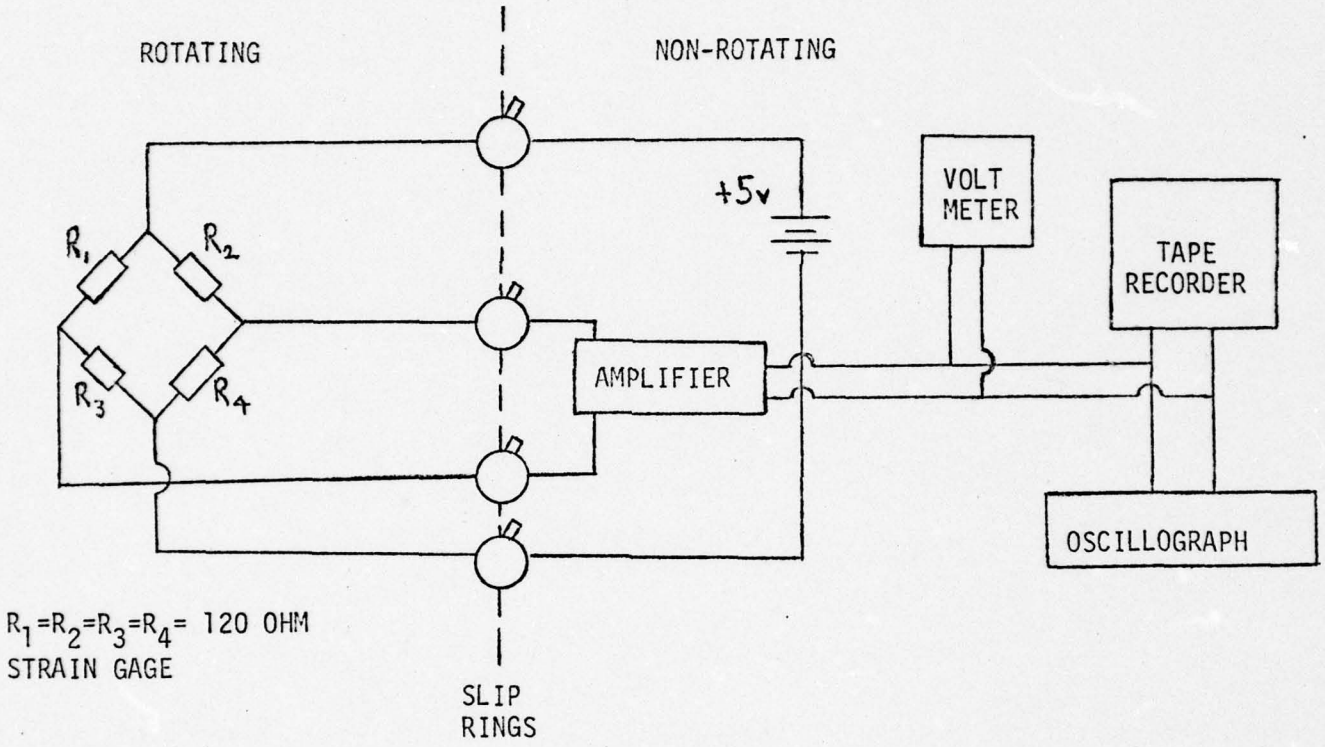

FIGURE 21 STRAIN GAGE BRIDGE SCHEMATIC

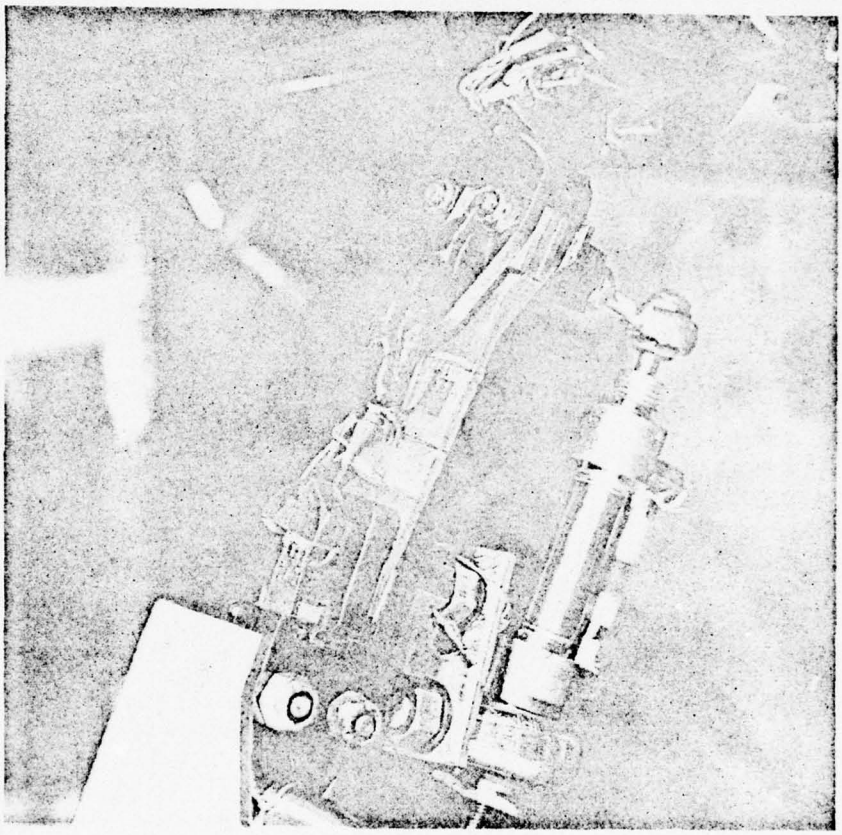

FIGURE 22 CHORDWISE, TORSIONAL, AND FLAPPING STRAIN GAGES

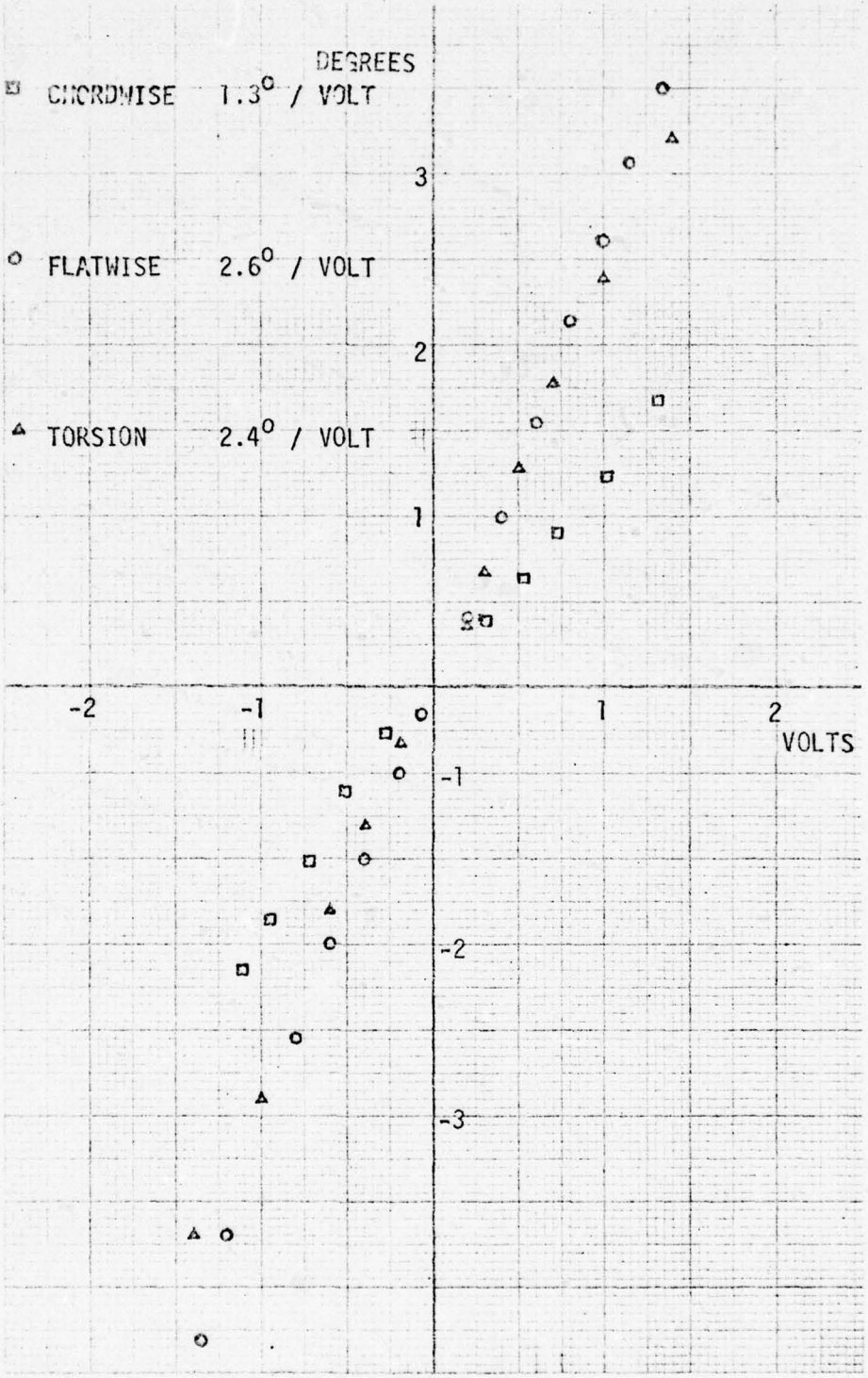

FIGURE 23 STRAIN GAGE CALIBRATION

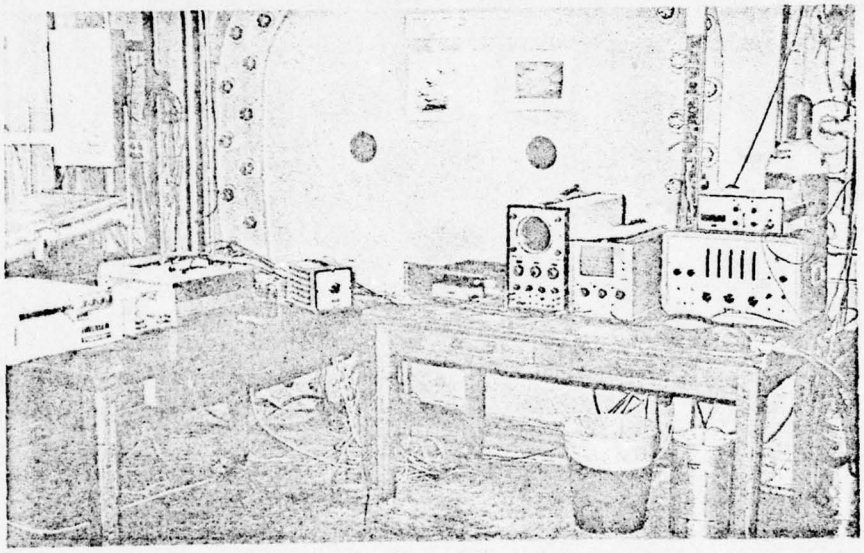

FIGURE 24 CONTROL INSTRUMENTATION IN
WRIGHT BROTHERS WIND TUNNEL

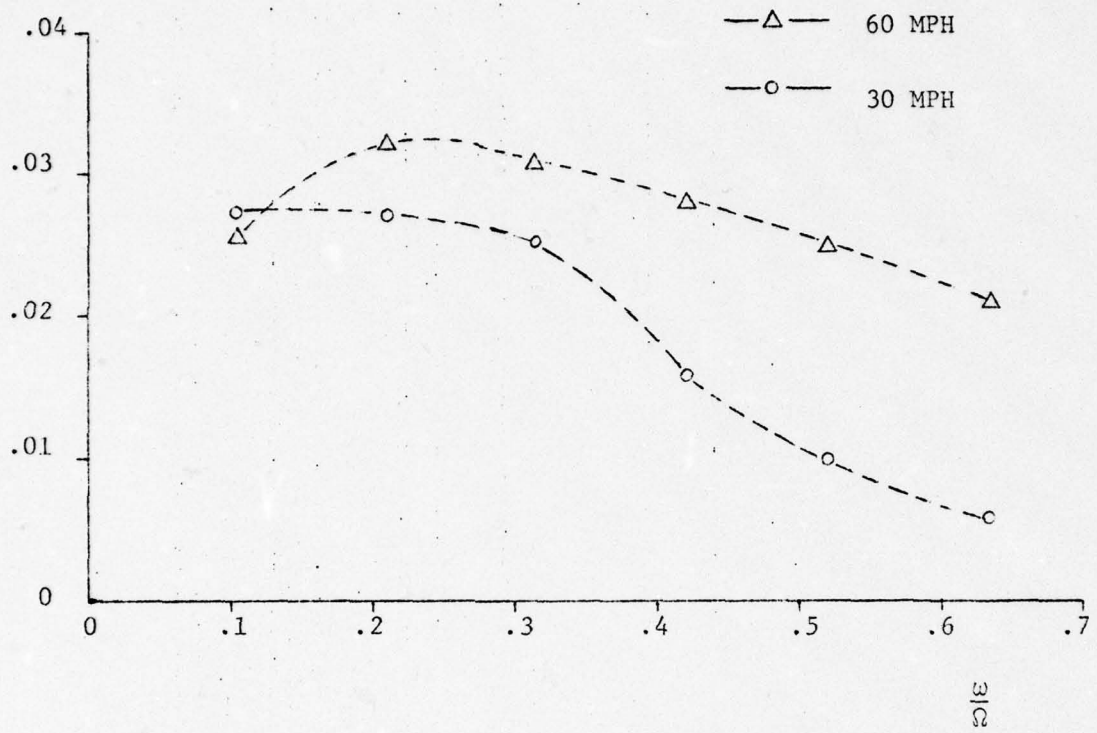

FIG. 25 GUST CALIBRATION, PLENUM PRESSURE = 4 PSI

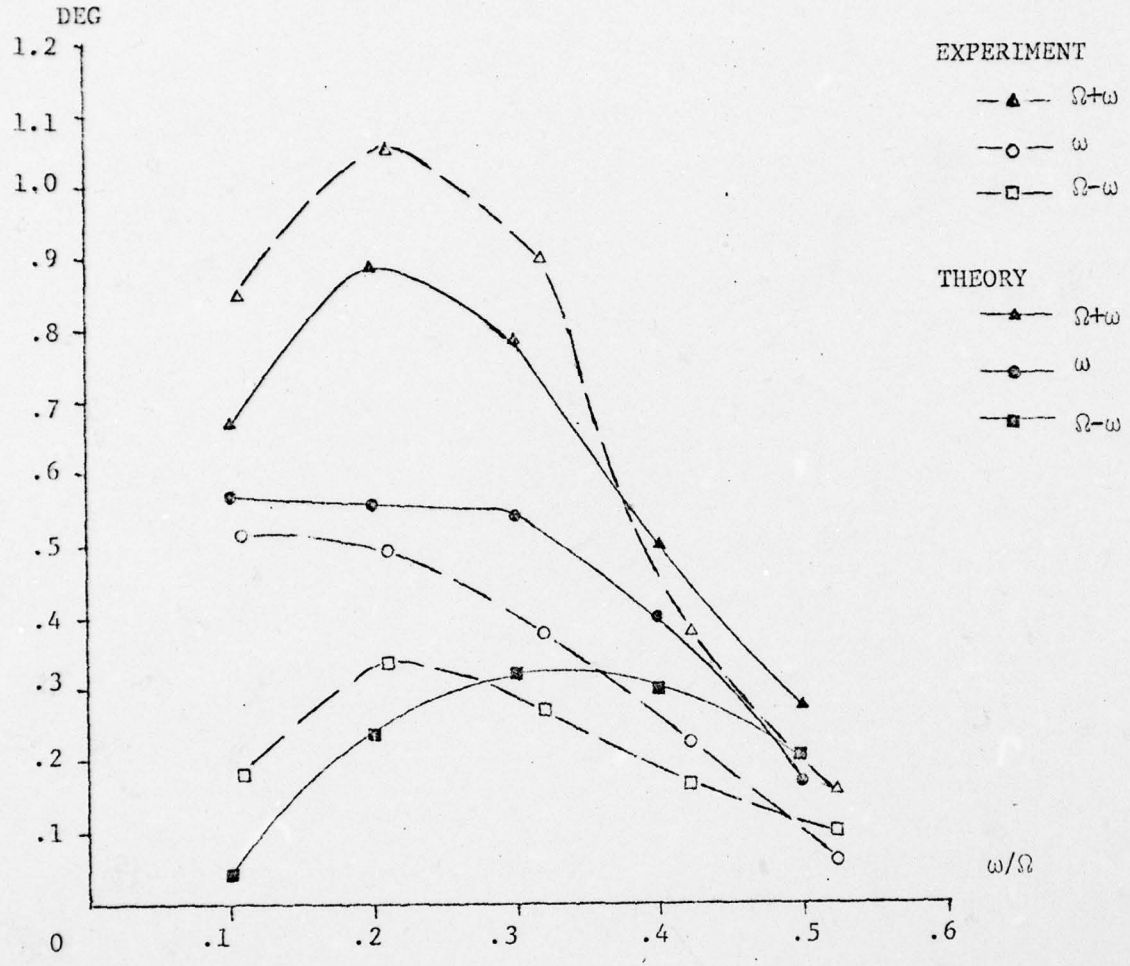

FIG. 26 THREE BLADED, 30 MPH, FLAP

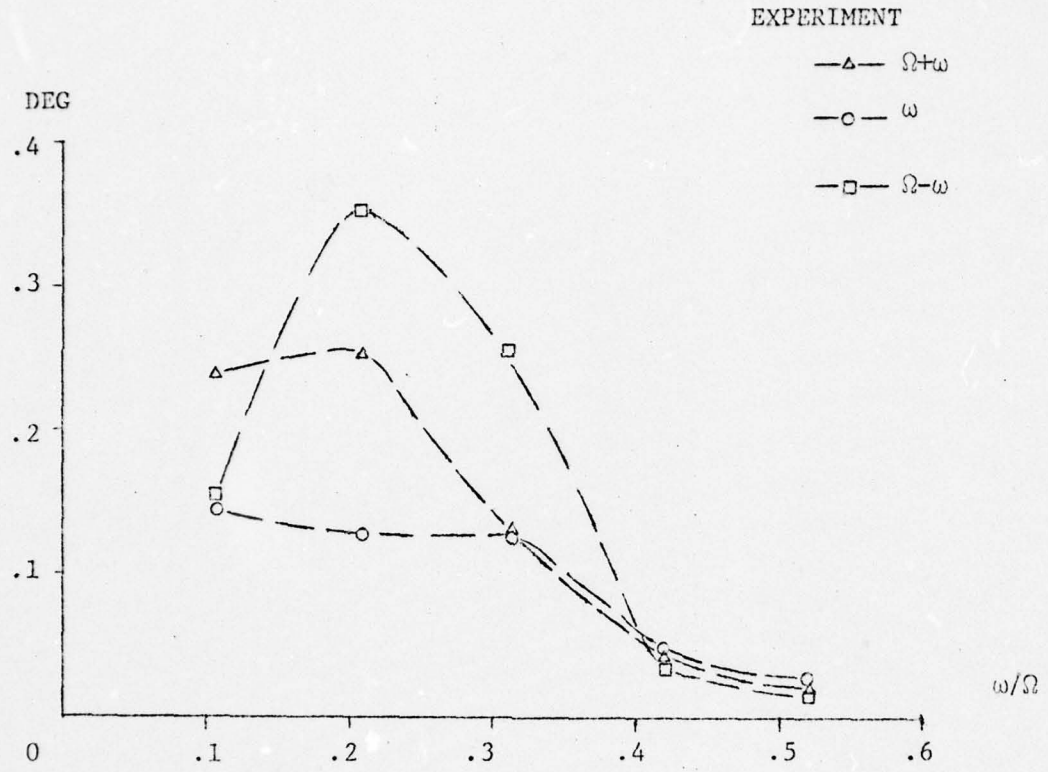

FIG. 27 THREE BLADED, 30 MPH, LAG

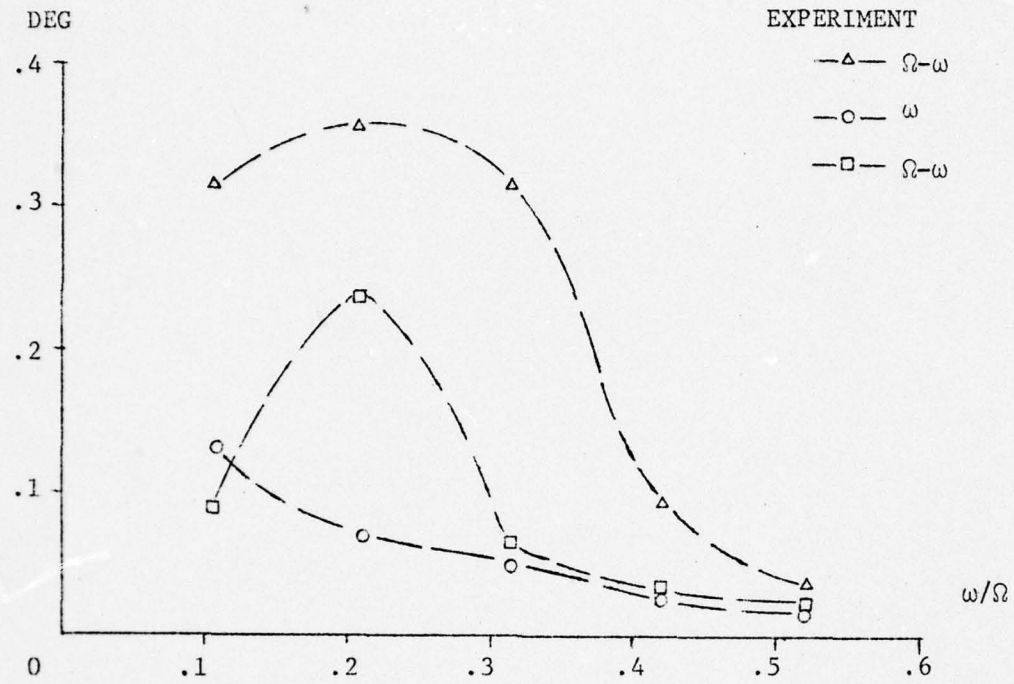

FIG. 28 THREE BLADED, 30 MPH, TORSION

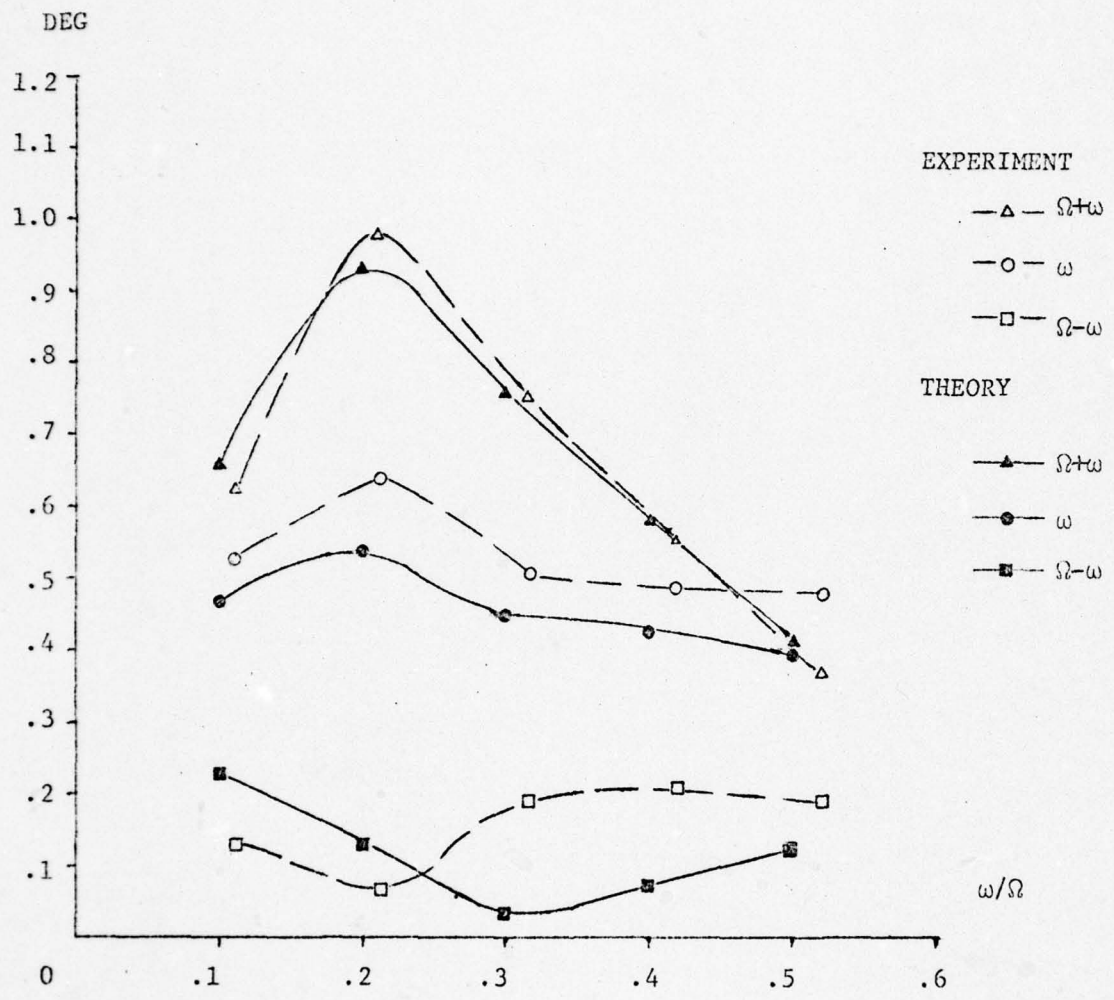

FIG. 29 THREE BLADED, 60 MPH, FLAP

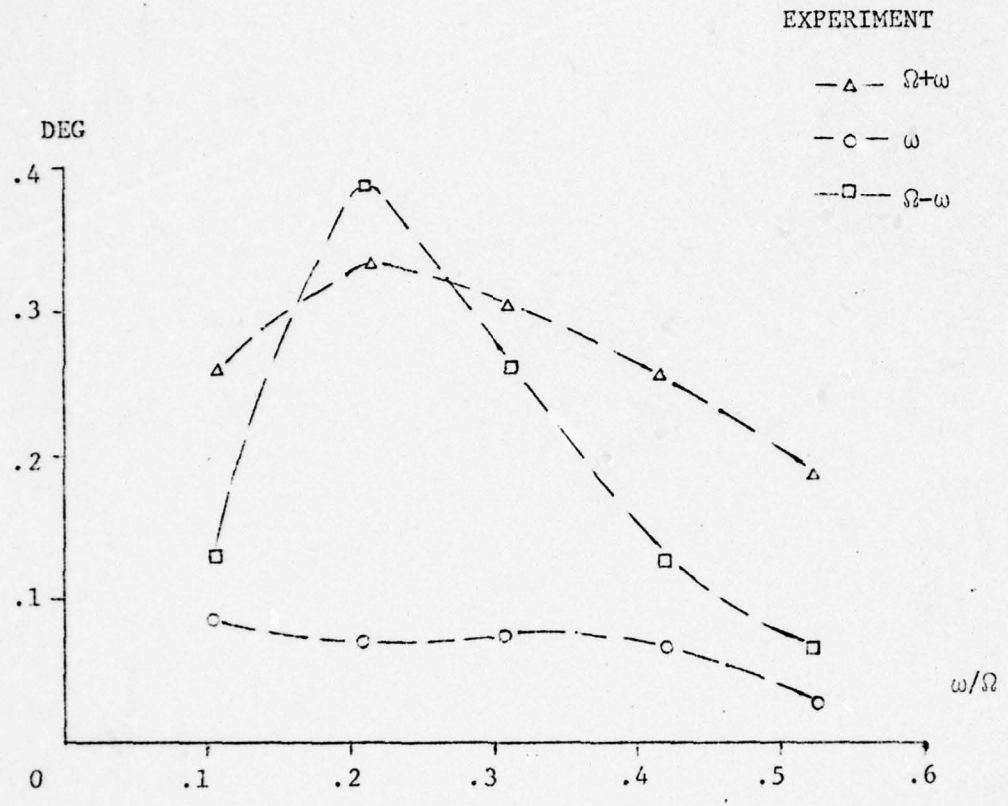

FIG. 30 THREE BLADED, 60 MPH, LAG

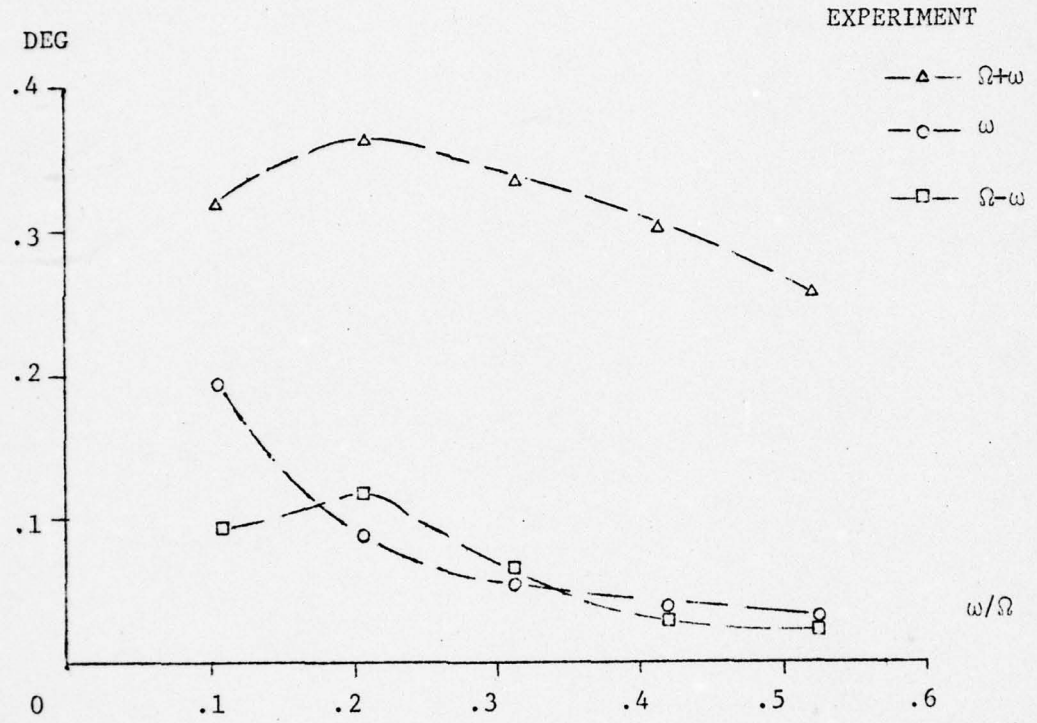

FIG. 31 THREE BLADED, 60 MPH, TORSION

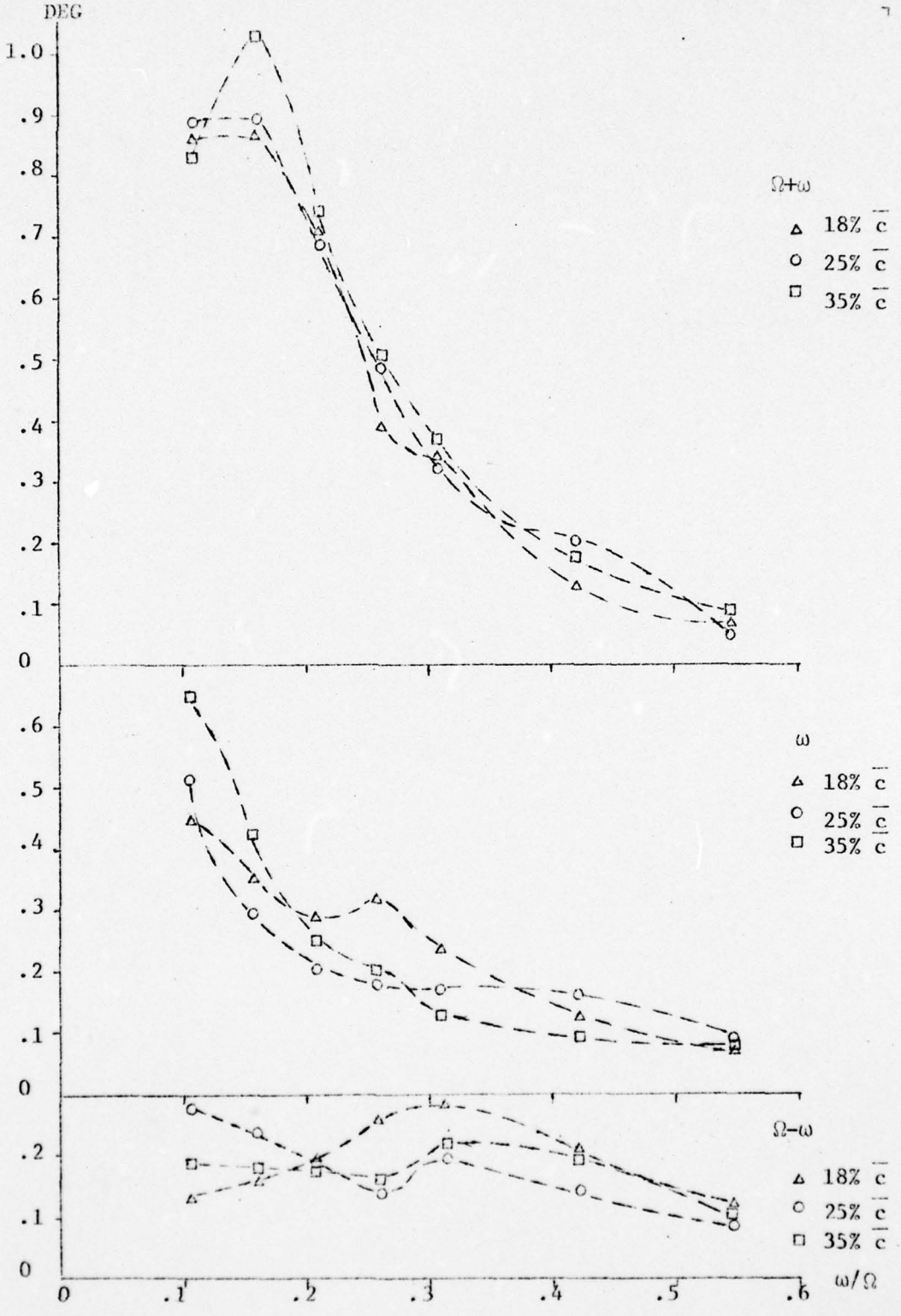

FIG. 32 SOFT FLEXURE, 30 MPH, FLAP

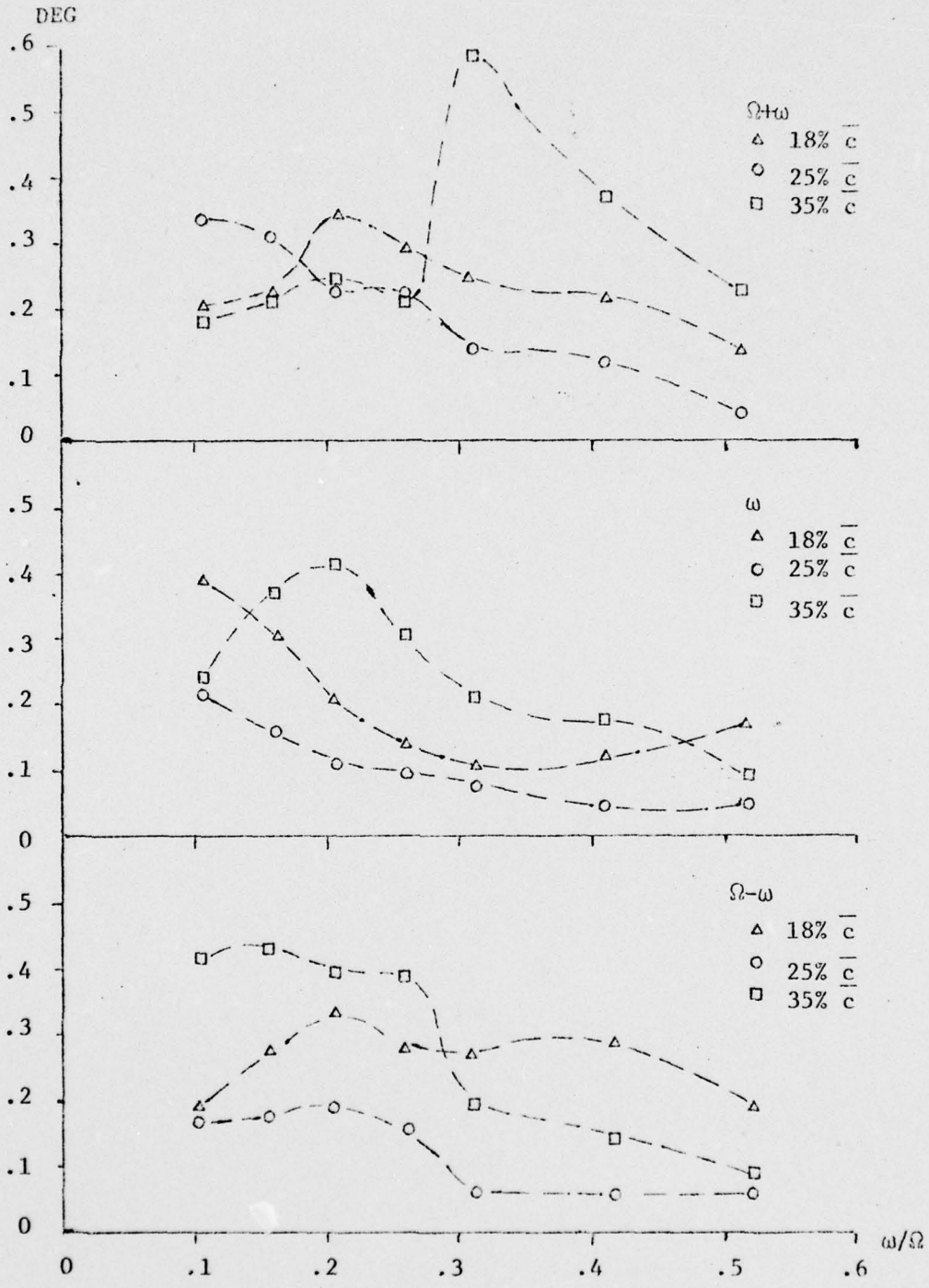

FIG. 33 SOFT FLEXURE, 30 MPH, TORSION

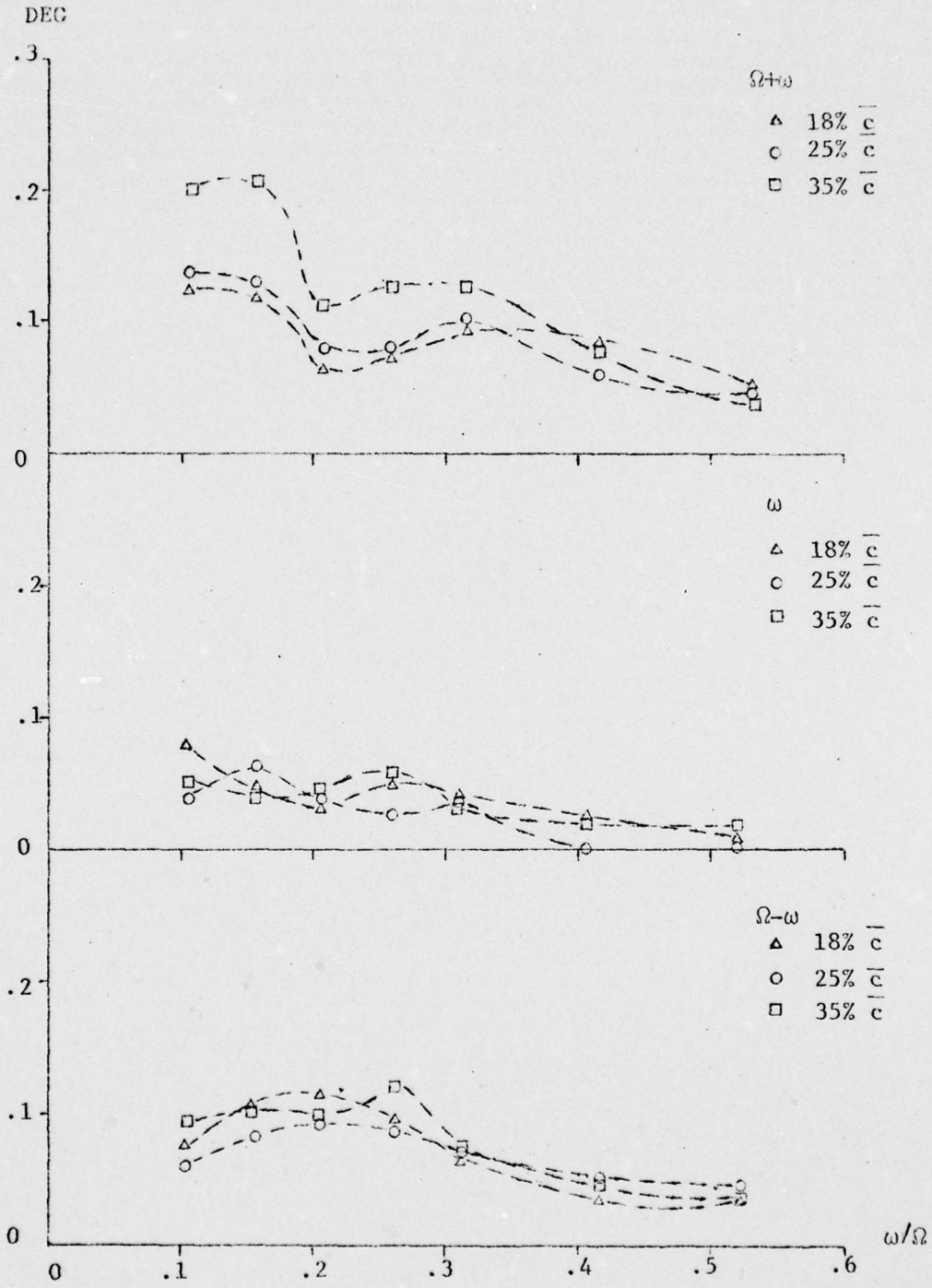

FIG. 34 SOFT FLEXURE, 30 MPH, LAG

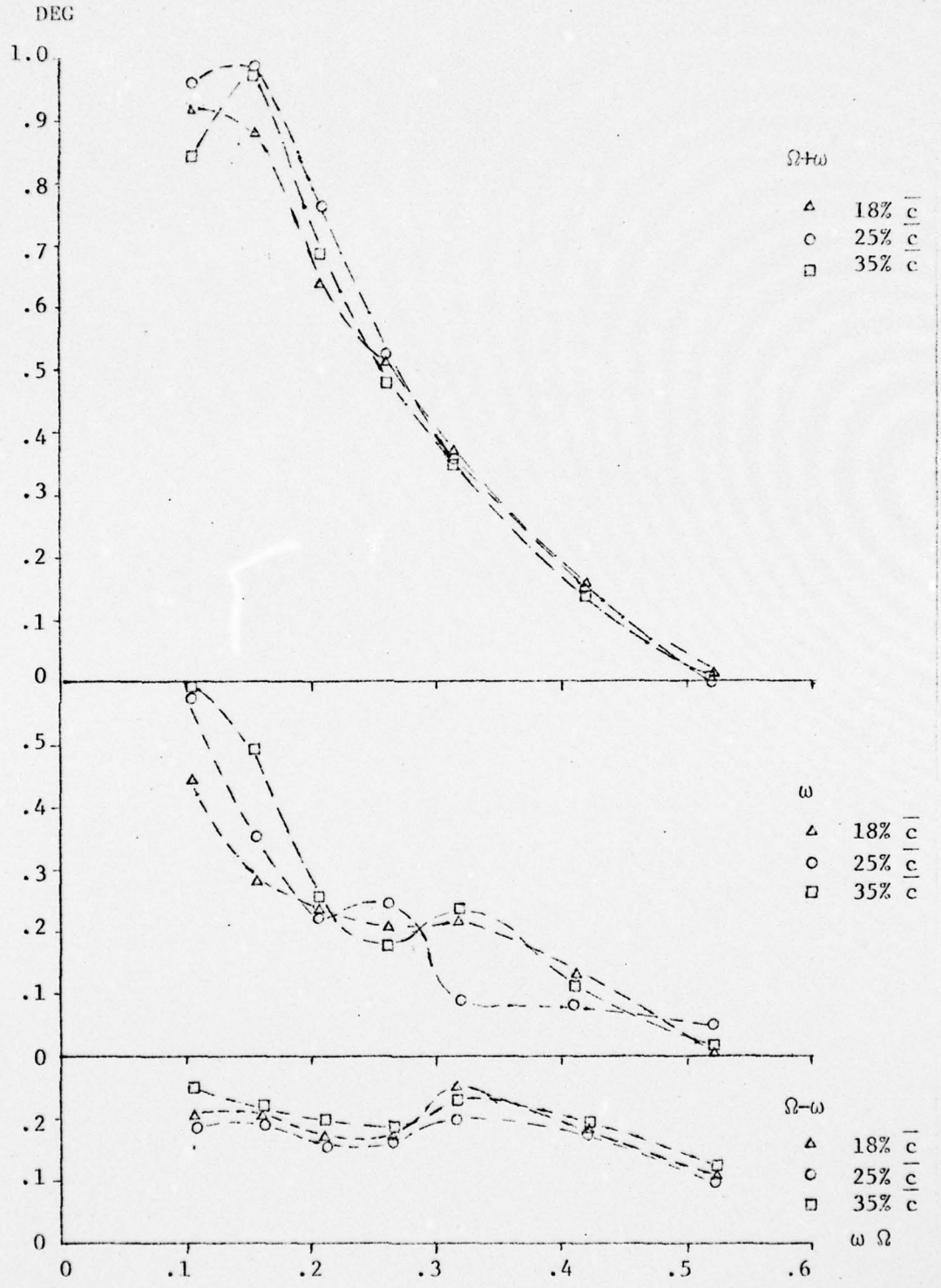

FIG. 35 STANDARD FLEXURE, 30 MPH, FLAP

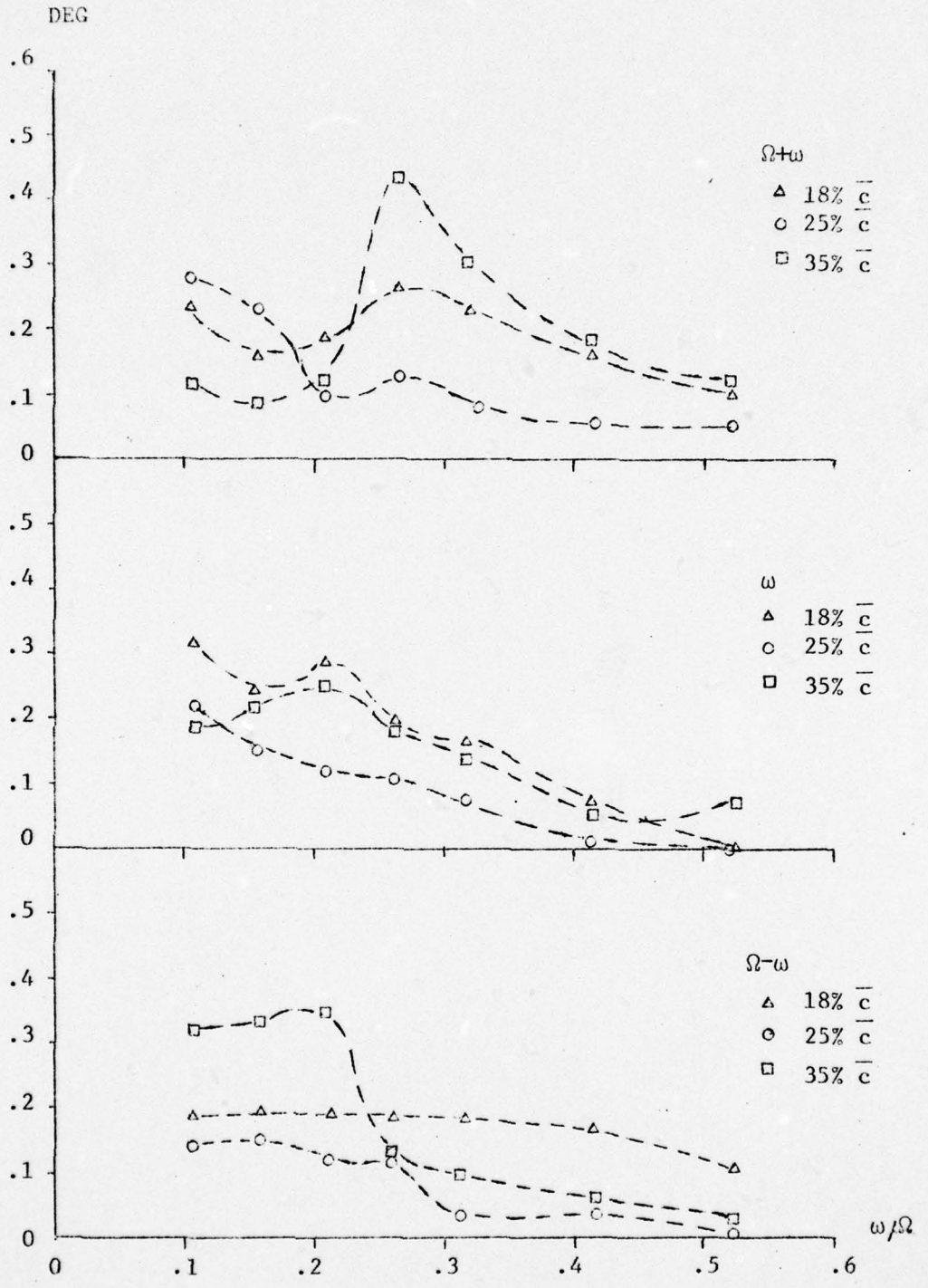

FIG. 36 STANDARD FLEXURE, 30 MPH, TORSION

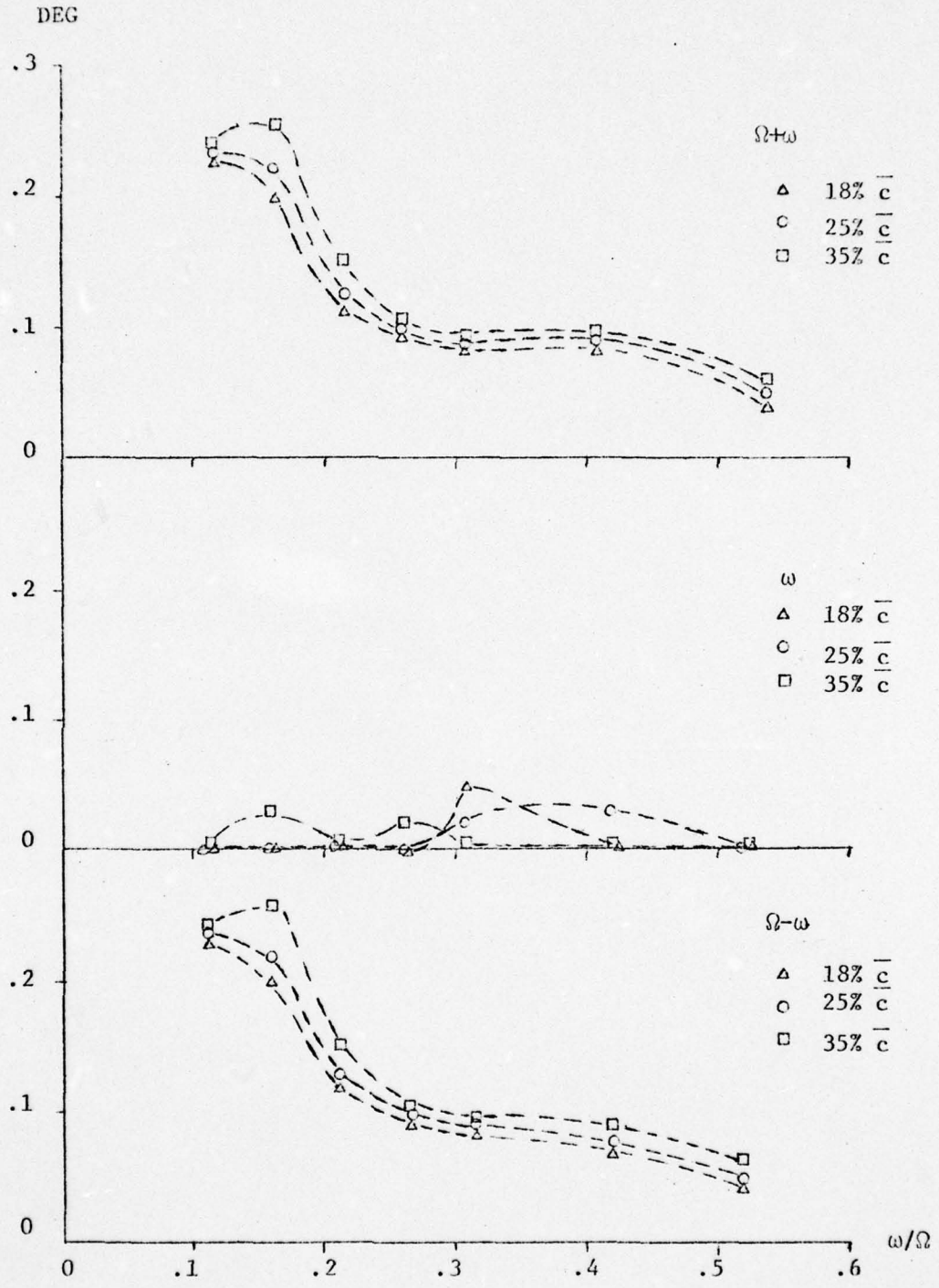

FIG. 37 STANDARD FLEXURE, 30 MPH, LAG

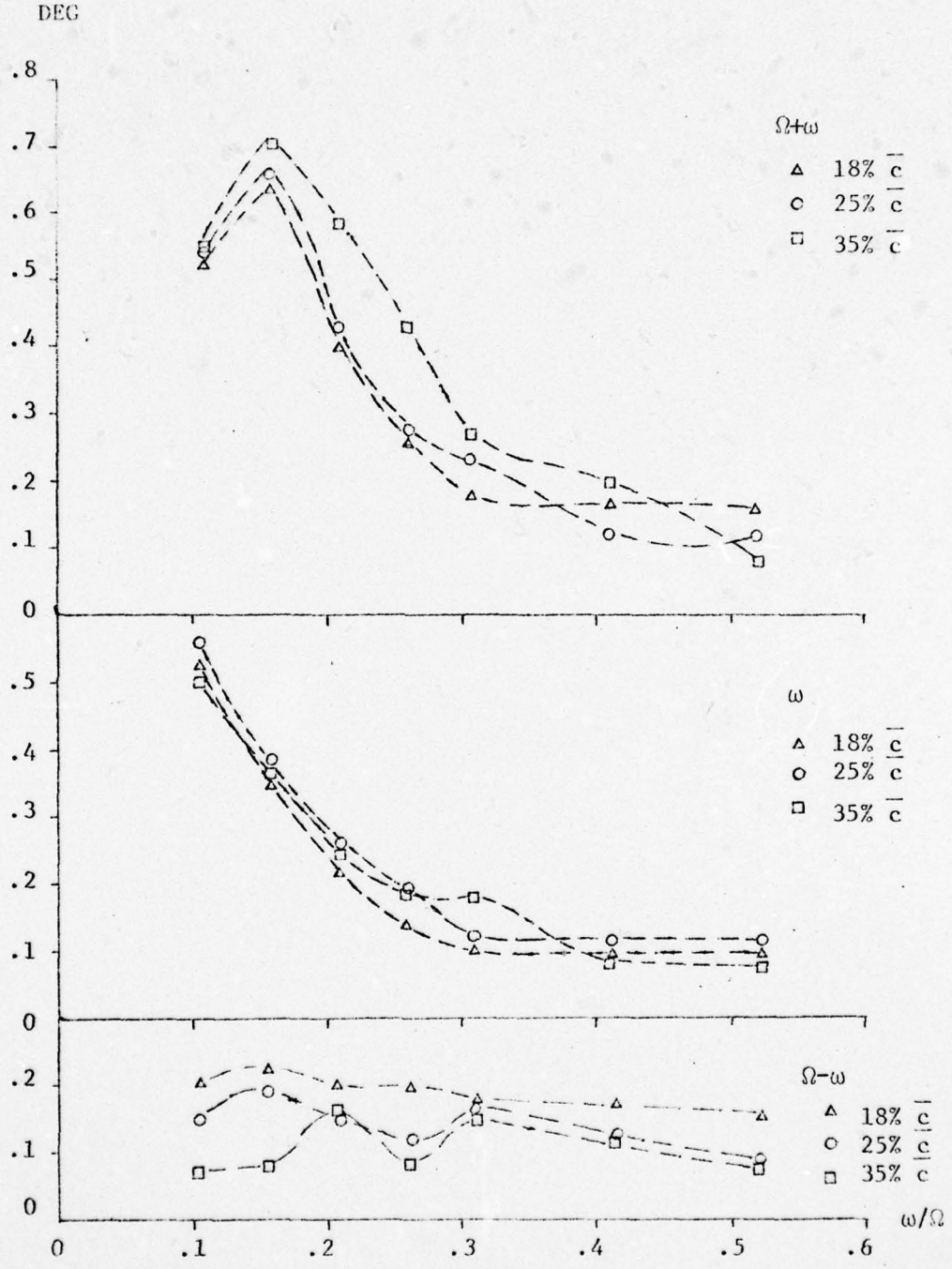

FIG. 38 STANDARD FLEXURE, 60 MPH, FLAP

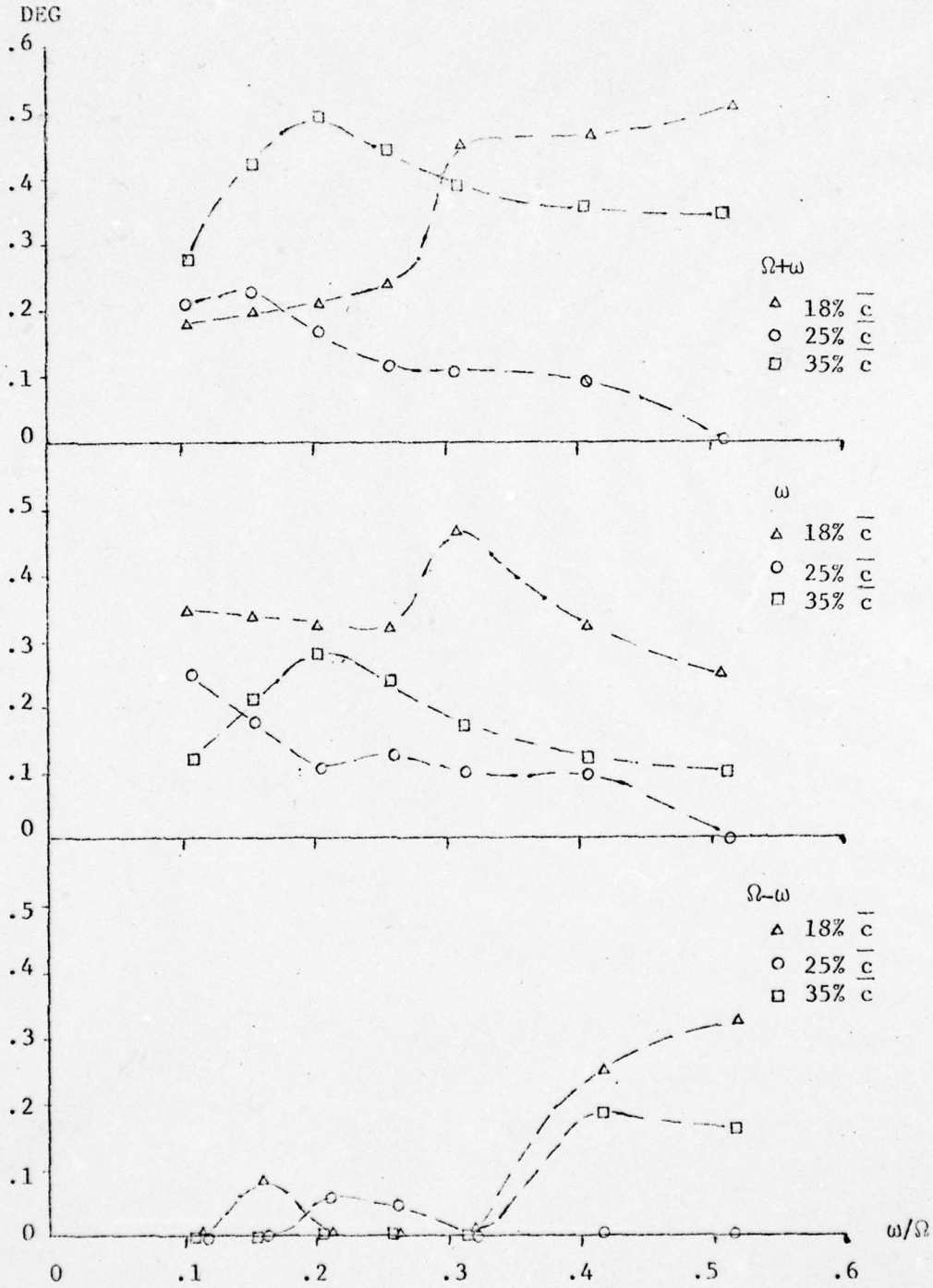

FIG. 39 STANDARD FLEXURE, 60 MPH, TORSION

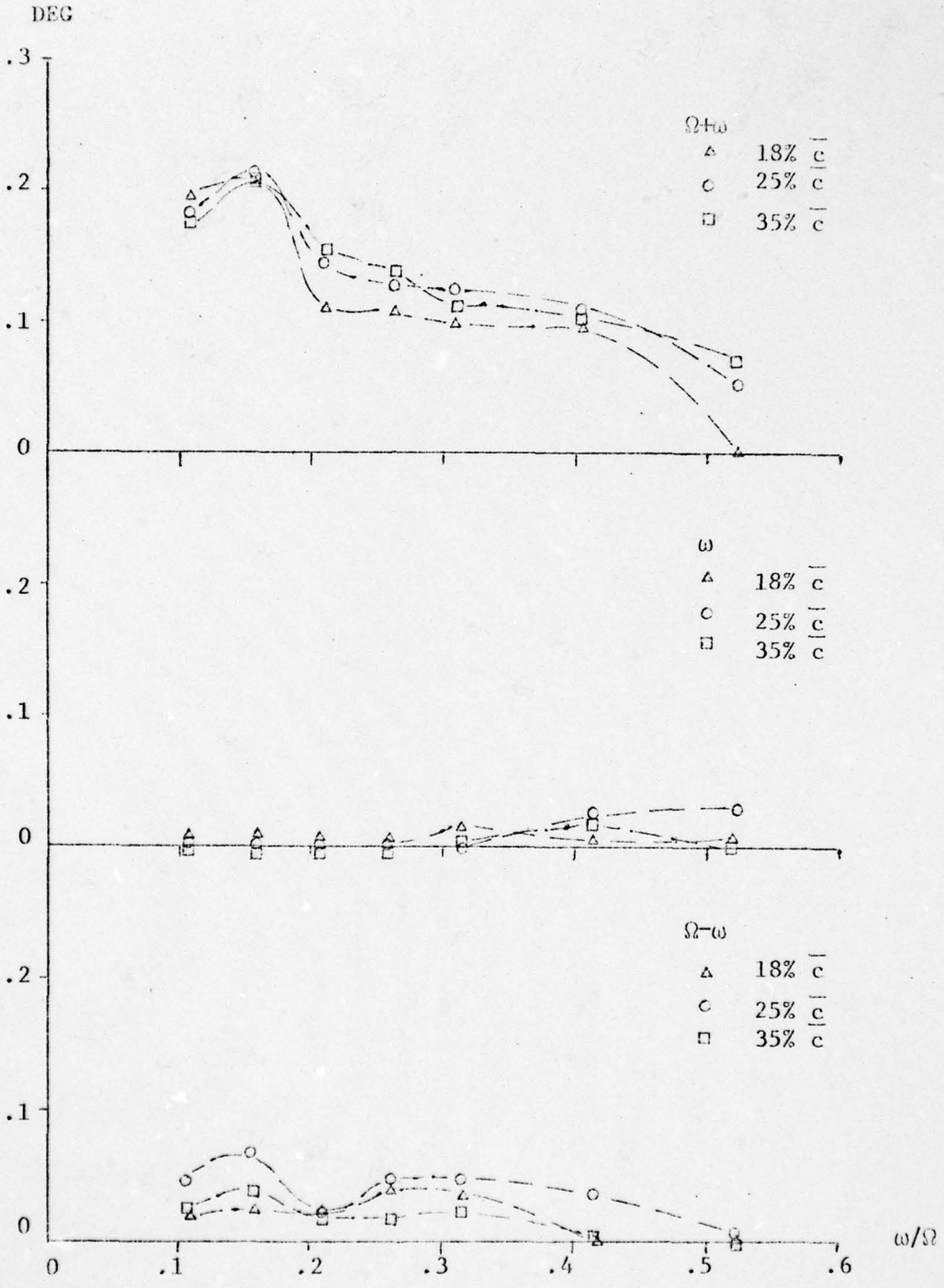

FIG. 40 STANDARD FLEXURE, 60 MPH, LAG

AD-A054 752 MASSACHUSETTS INST OF TECH CAMBRIDGE DEPT OF AERONAU--ETC F/G 1/3
EXPERIMENTAL INVESTIGATION OF GUST RESPONSE OF HINGELESS HELICO--ETC(U)
JUN 77 C A VEHLOW

UNCLASSIFIED NL

2 OF 2
AD
A054752

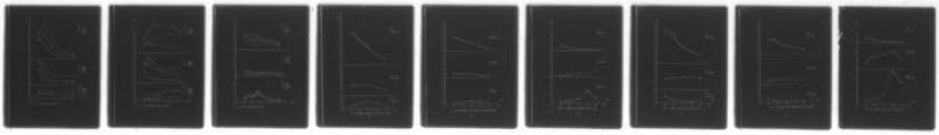

END
DATE FILMED
7-78
DDC

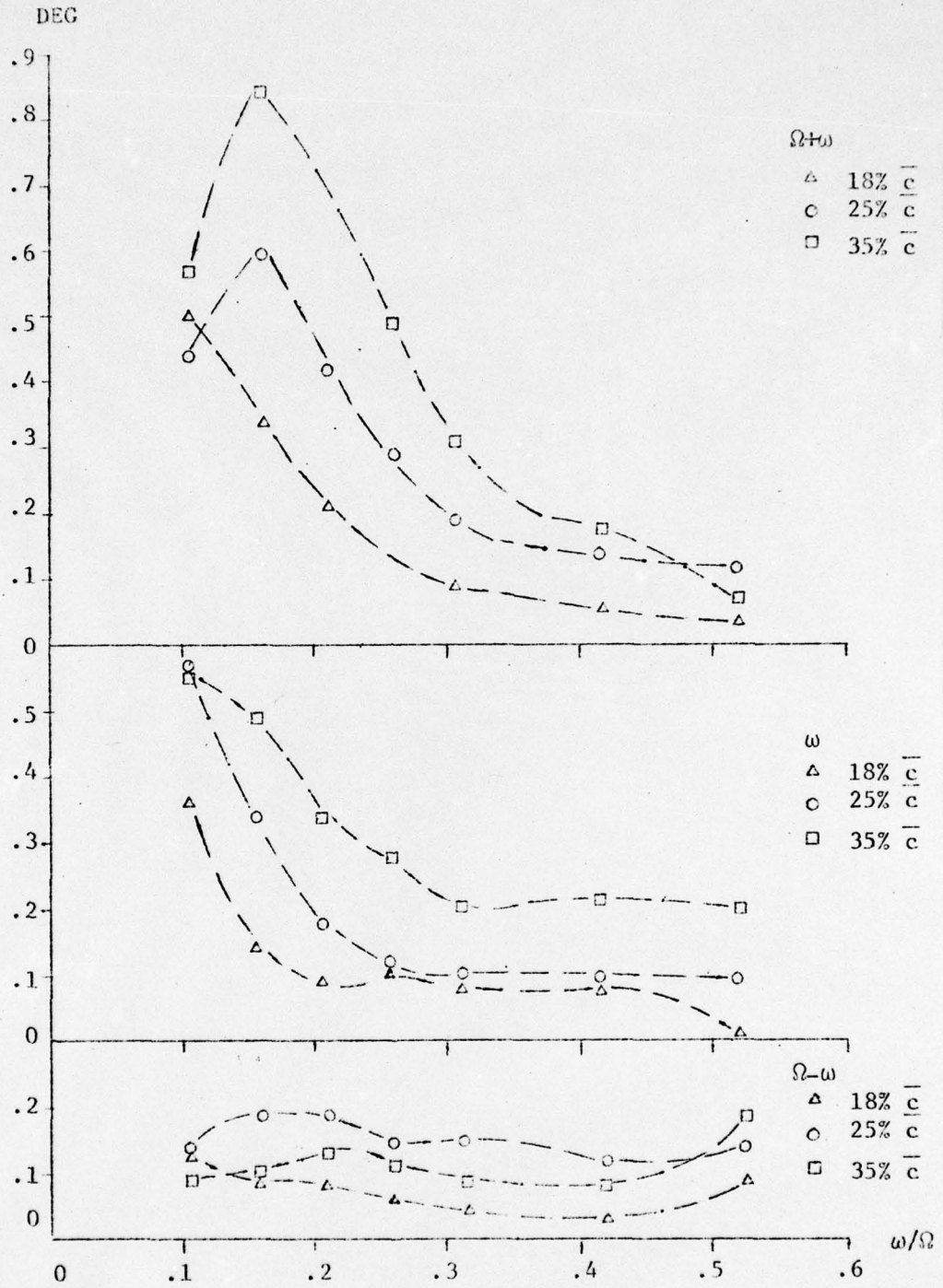

FIG. 41 SOFT FLEXURE, 60 MPH, FLAP

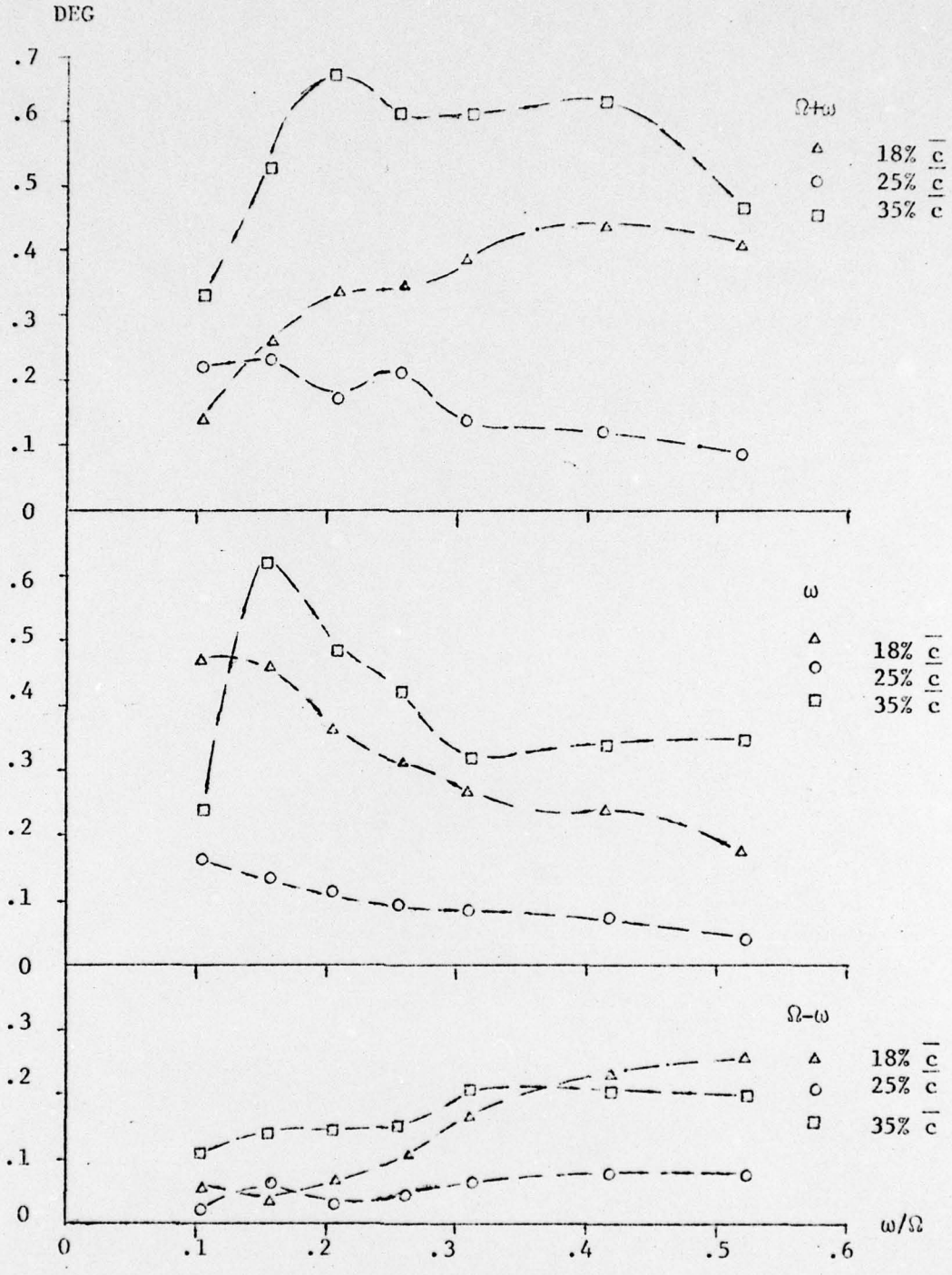

FIG. 42 SOFT FLEXURE, 60 MPH, TORSION

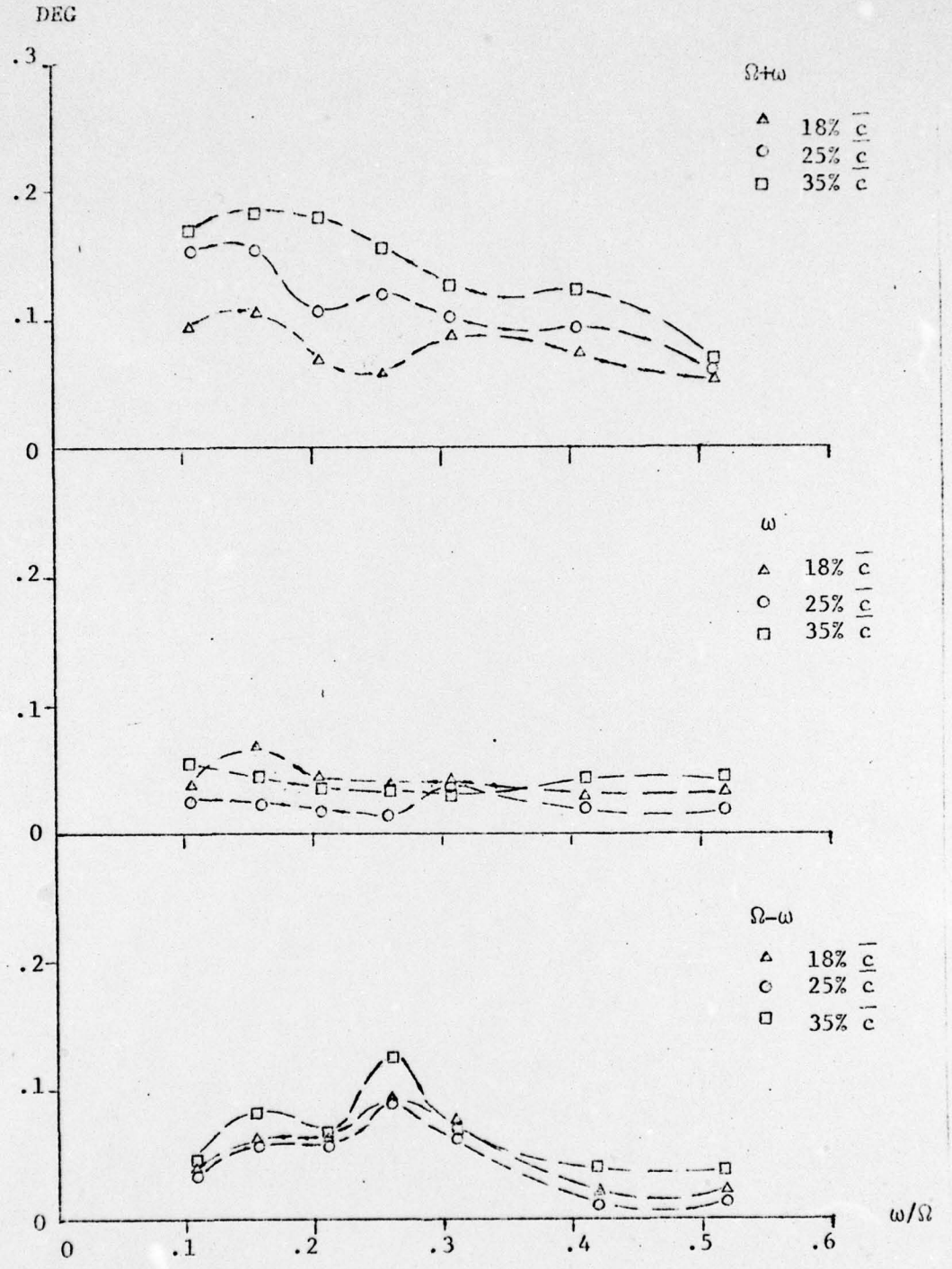

FIG. 43 SOFT FLEXURE, 60 MPH, LAG

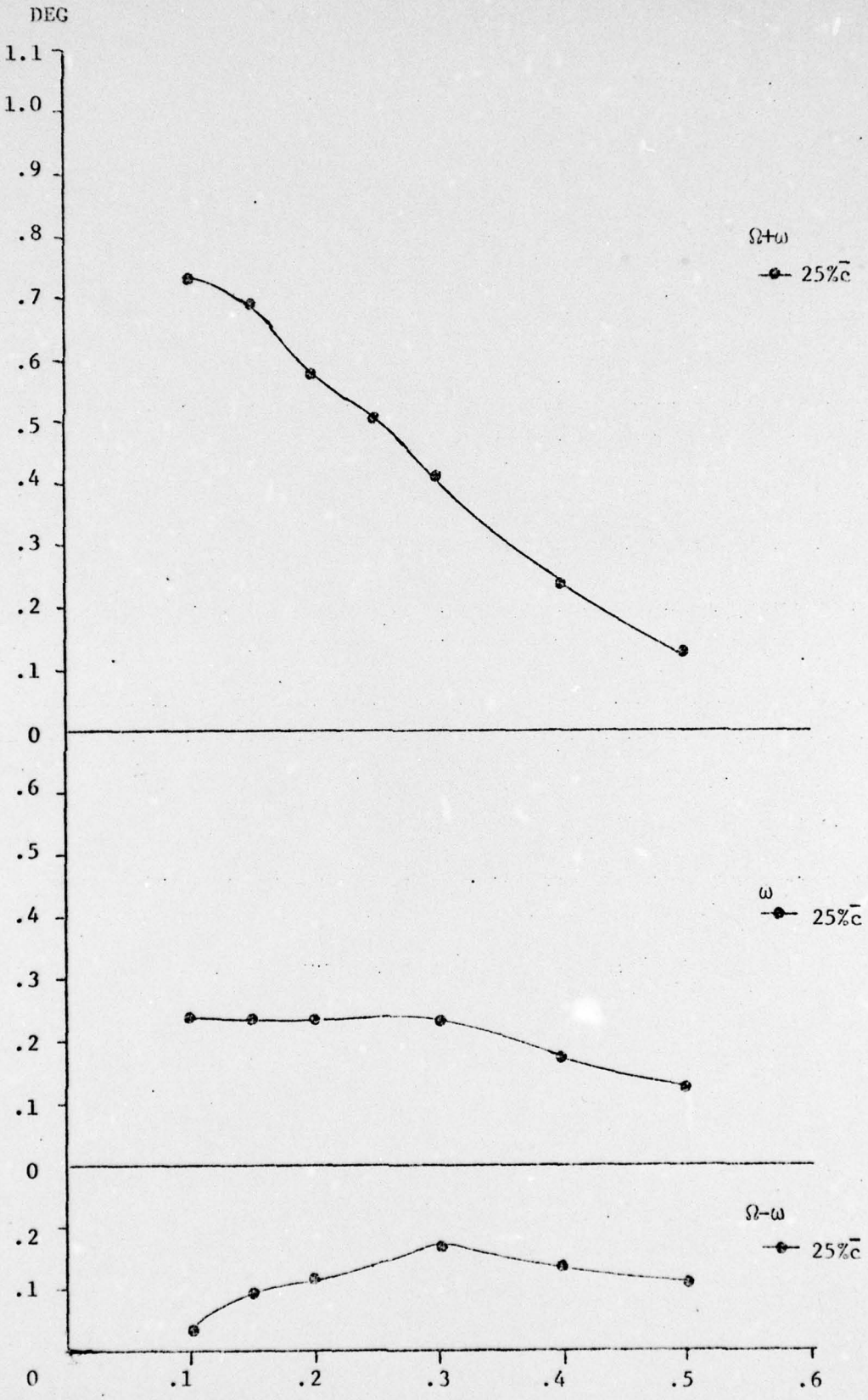

FIG. 44 THEORY, SOFT FLEXURE, 30 MPH, FLAP

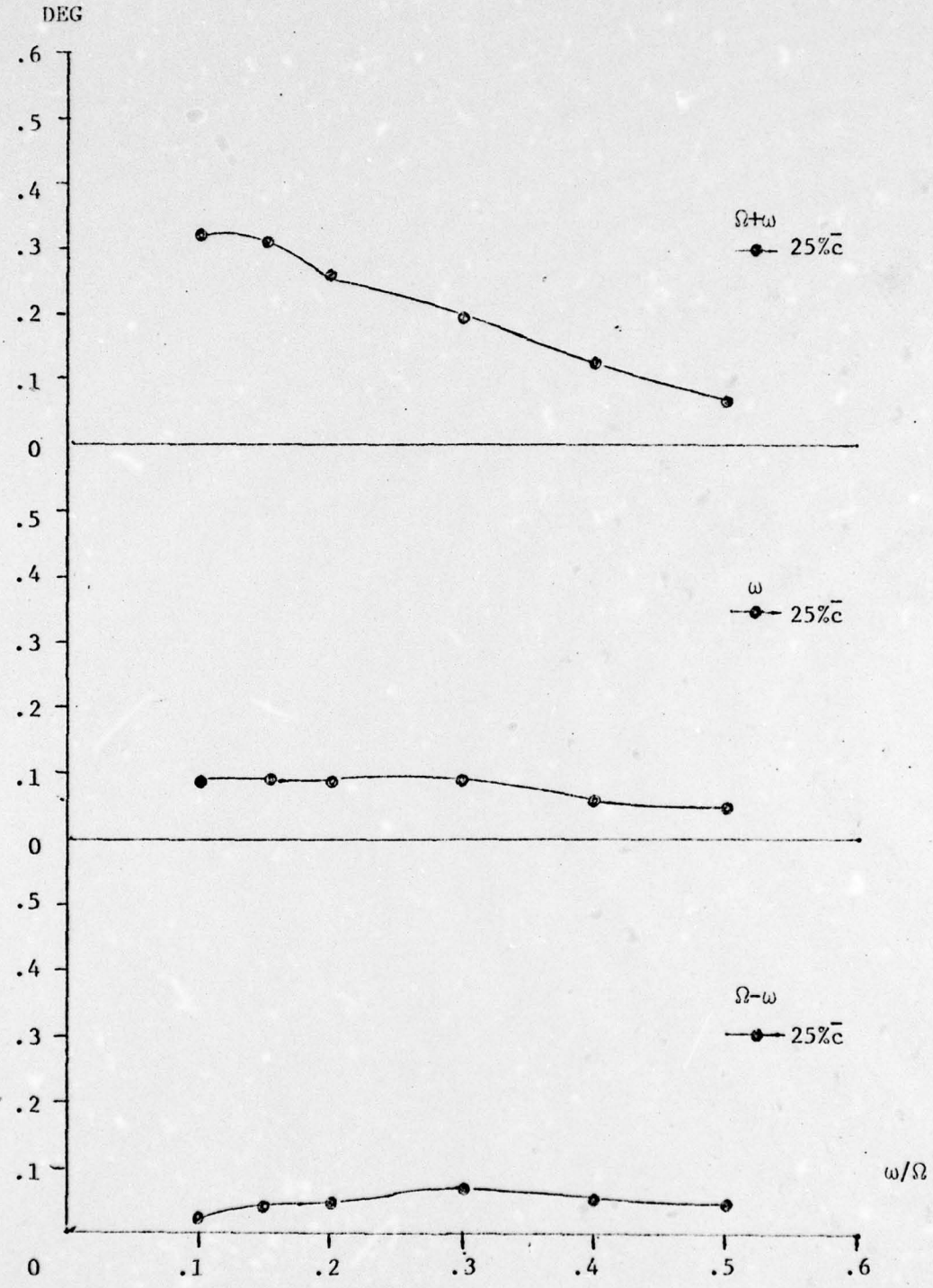

FIG. 45 THEORY, SOFT FLEXURE, 30 MPH, TORSION

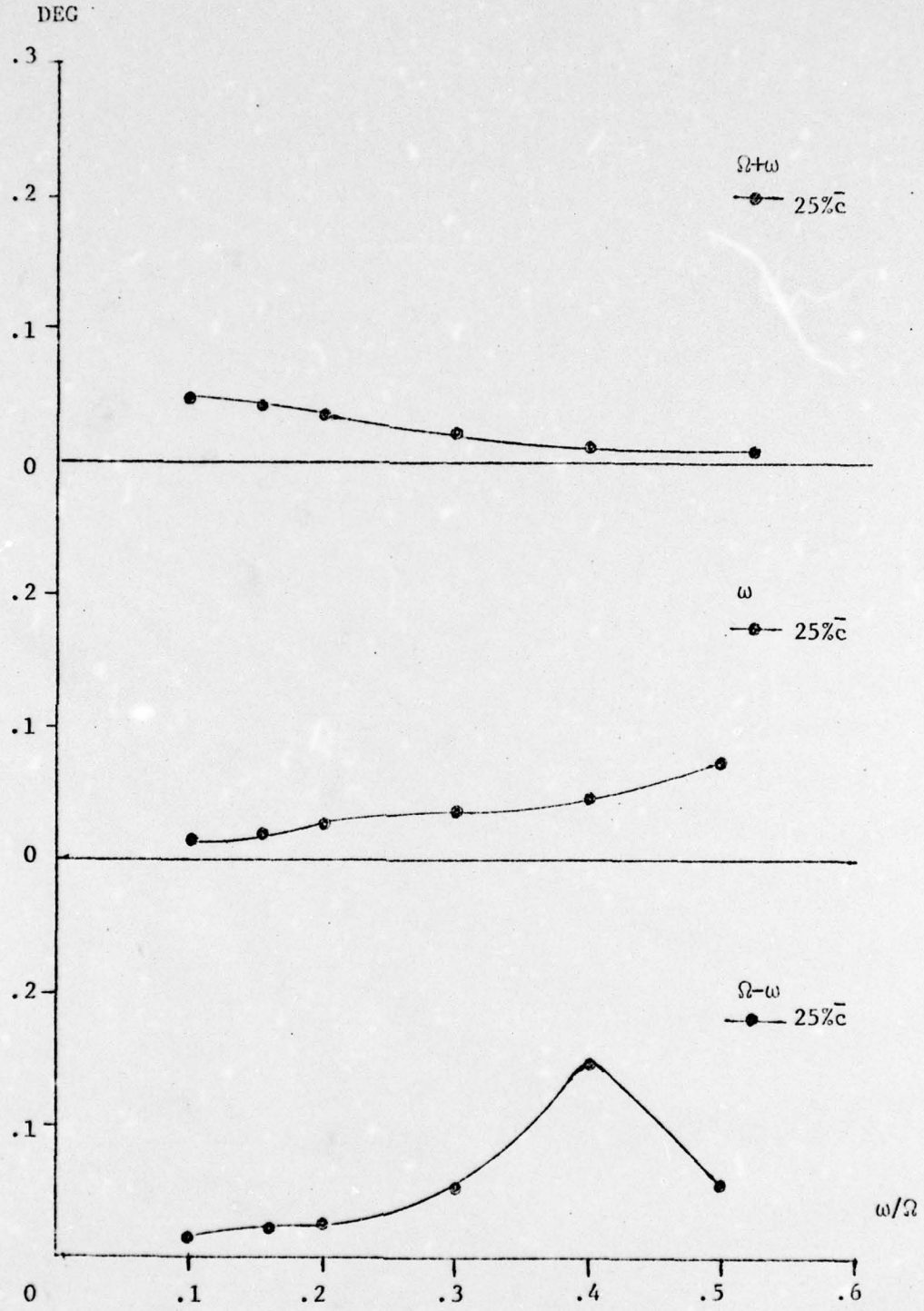

FIG. 46 THEORY, SOFT FLEXURE, 30 MPH, LAG

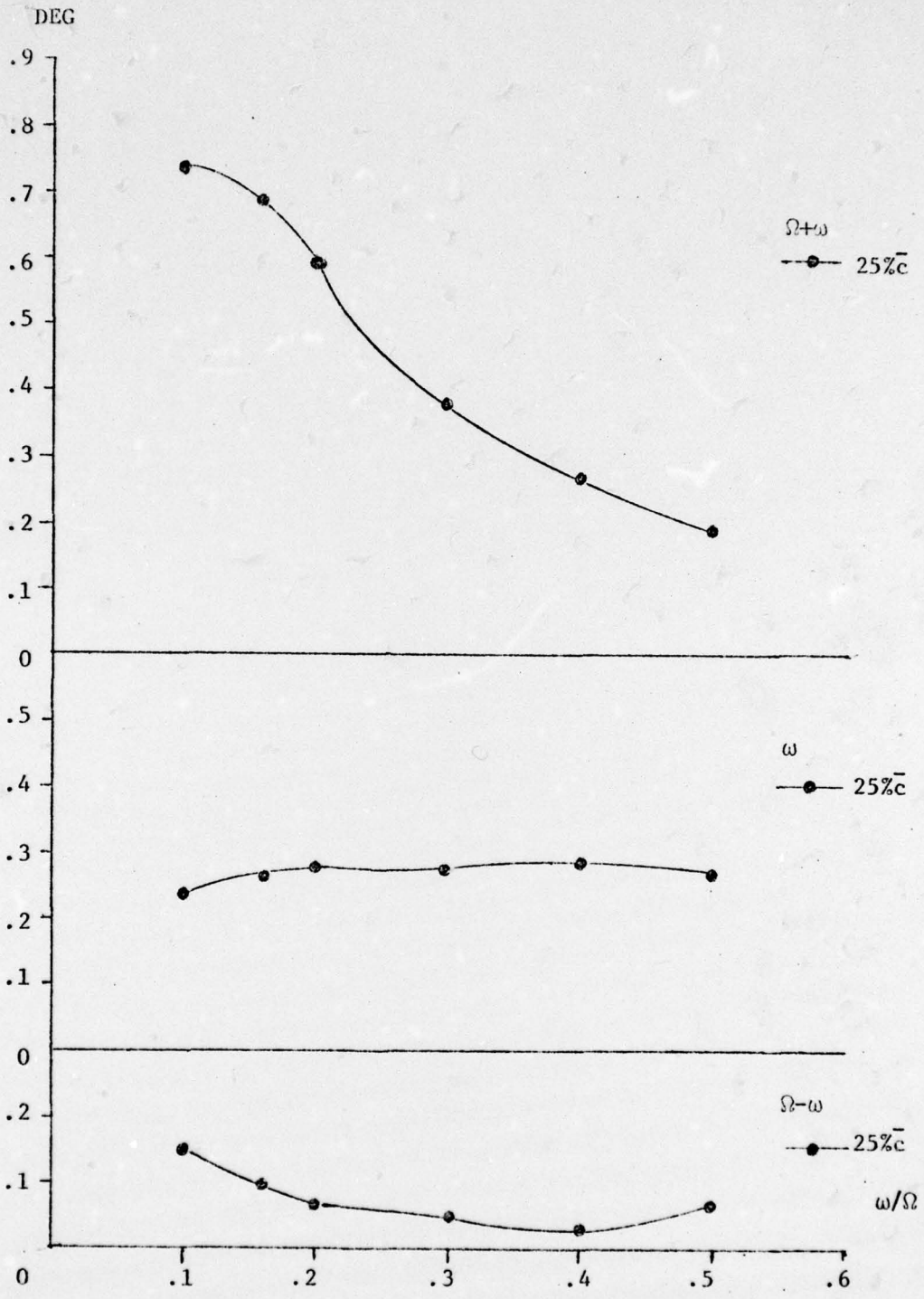

FIG. 47 THEORY, SOFT FLEXURE, 60 MPH, FLAP

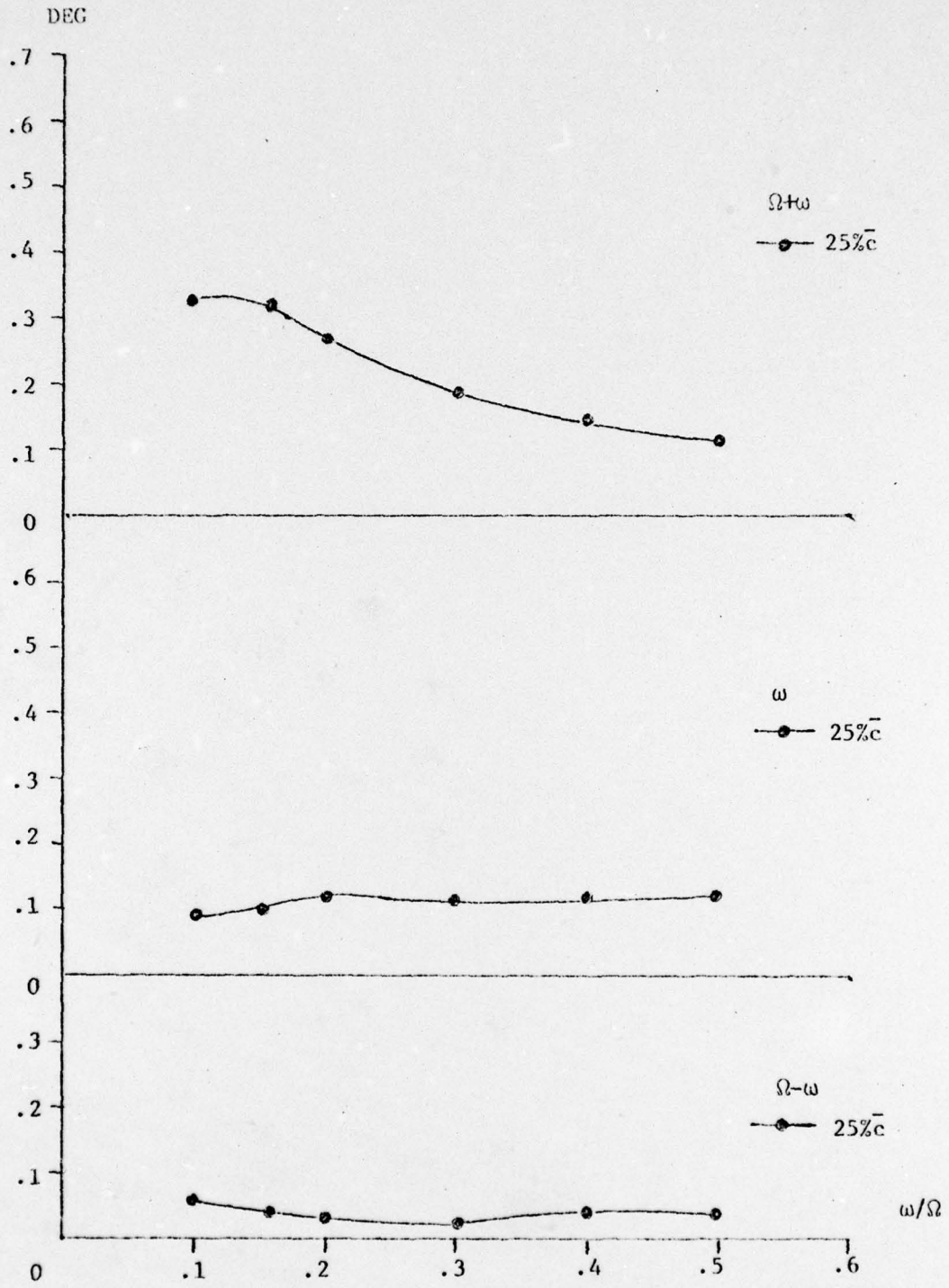

FIG. 48 THEORY, SOFT FLEXURE, 60 MPH, TORSION

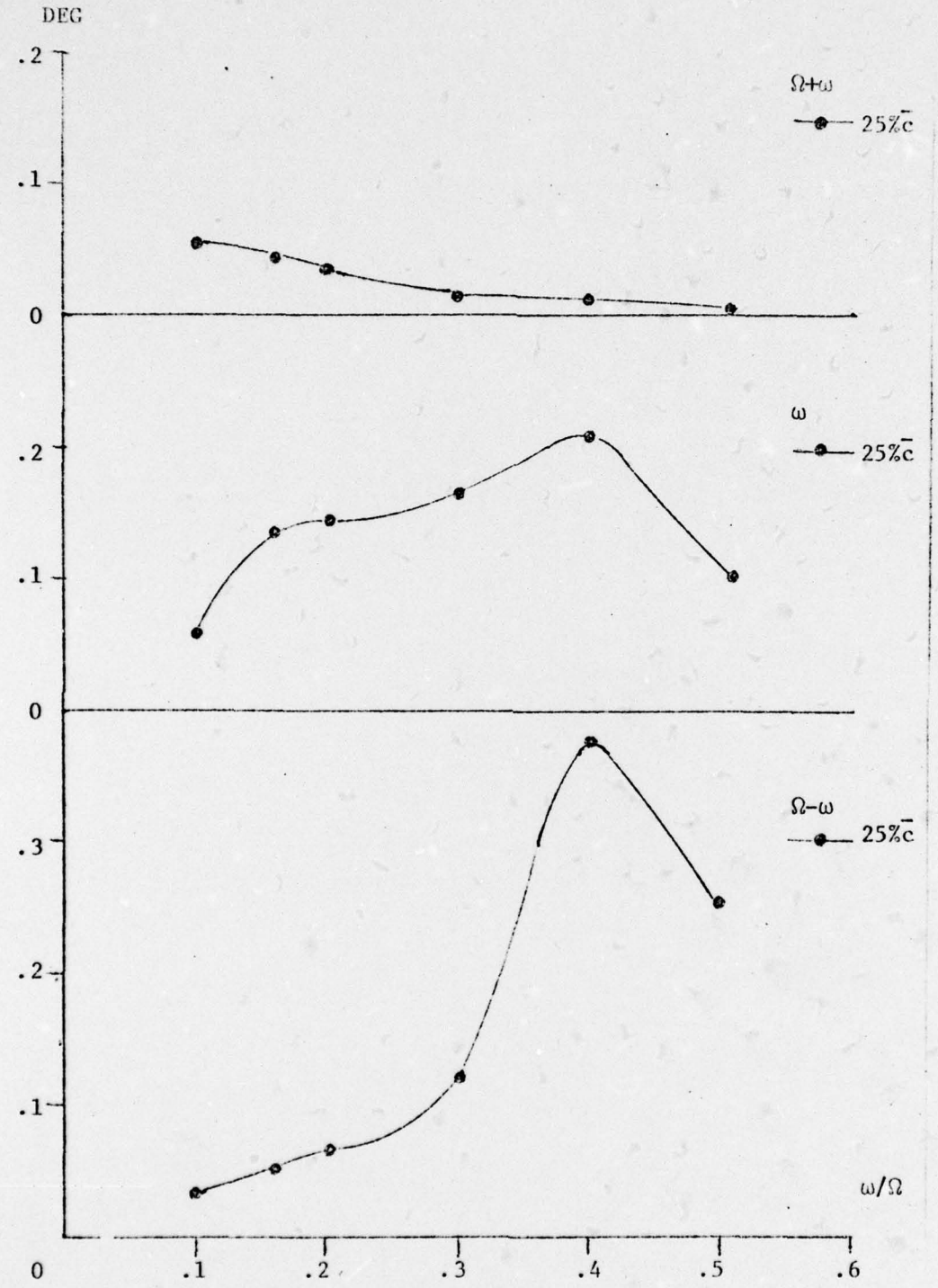

FIG. 49 THEORY, SOFT FLEXURE, 60 MPH, LAG